Unbalanced Current Sharing Control in Islanded Low Voltage Microgrids

Foad Najafi[1] * and Matthias Fripp[1]

[1] Department of Electrical Engineering, University of Hawaii at Manoa, Honolulu, Hawaii, 96822
* Correspondence: fnajafi@hawaii.edu

Abstract: In this paper, a new control strategy for power management improvement of islanded LV microgrids is proposed. The controllers are designed in the stationary frame. The control structure consists of four loops; 1) the current controller; 2) the voltage controller; 3) the droop controller and the 4) negative and zero sequence current controllers. The output current is considered unknown for the controller and is added to the control system as a disturbance. The proposed controller features a high gain in fundamental and harmonic frequencies, hence a good voltage quality is obtained in the presence of unbalanced and nonlinear loads. To this aim, a proportional-resonant (PR) controller is adopted as the current controller. By using a multi-resonant controller as current controller, a unified control structure is obtained which is suitable for both grid-connected and islanded modes. The voltage controller is designed using a resonant controller so that the voltage can have low VUF and THD in the presence of unbalanced and nonlinear loads. Furthermore, in this paper droop method is applied to the control structure to share real and reactive powers. Simulation studies show that the conventional droop method cannot share the oscillatory part of the output power that is due to the presence of unbalanced loads in the microgrid. This paper relies on using zero and negative sequence virtual impedance controller to share the oscillatory part of output power. By using zero-sequence virtual impedance controller (ZSVIC) and negative-sequence virtual impedance controller (NSVIC), the zero and negative sequence currents in the microgrid are controlled and shared effectively. By compensating zero- and negative-sequence currents locally, the flow of these currents in the microgrid is minimized, and the overall power quality of the islanded LV microgrid is improved.

Keywords: Distributed generation, LV microgrid, negative-sequence current, zero-sequence current, power sharing, unbalance load, voltage control.

1. Introduction

Distributed energy resources (DERs) are small power sources to provide the required power to meet the increasing demand. Different power quality issues are appeared after placing DERs [1,2]. Various research works have been performed to deal with these matters. Microgrids are small-scale power systems with local resources (DERs) for production, consumption, and storage, that can work connected to the main grid or islanded [3]. An improved indicator was proposed in [4] to estimate the voltage stability margin of a two-bus system based on both saddle-node and limited induced bifurcations. A new concept named reduced islanded microgrid network was used for generalization of the proposed index ton-bus islanded microgrids and a development power flow algorithm by splitting these networks. Consideration of the system maximum loadability, a droop-controlled based method was proposed in [5] in islanded microgrids for optimal power flow problems. An optimal control algorithm was presented in [6] for DERs to improve the power quality and reduce the energy costs of a hybrid AC-DC microgrid. Authors in [7] proposed a control method based on Lyapunov control theory to investigate the stability of the DG units while operating alongside the utility grid.

In [8], The passivity-based control technique is utilized to analyze the dynamic and steady-state behavior during integration with the power grid. By applying this technique, the harmonic and reactive power component can be supplied with a fast dynamic response. Power quality issues are

among the most challenging topics of controlling microgrids, especially in the islanded mode. Power quality problem consists of two main type: nonlinear and unbalances load. The proliferation of single-phase and nonlinear loads in the microgrids has made important challenges regarding the power quality of these networks [9]. In the grid-connected mode, if the microgrids cannot manage to compensate the current absorbed by nonlinear and unbalanced loads easily, the main grid can easily offset these currents. However, in the islanded mode, the microgrid itself is due to compensating the currents absorbed by nonlinear and unbalanced loads. In the islanded microgrids, power-sharing is more important compared to the grid-connected microgrids due to the limited capacity of the DG units hosted by the islanded microgrid in particular in the presence of unbalanced and harmonic loads [10].

When unbalance current increases proportional to the total current of the system, the voltage unbalances on some part of the system emerges[11]. Since the total capacity of islanded microgrid is limited, a small portion of single loads can make islanded microgrid severely unbalanced.

The problem that zero and negative sequence current create are [12]: 1: Increase the loss in the system, therefore increase the temperature in induction motors and transforms. 2: Vibrating induction motors which cause mechanical tension which reduces the lifetime of electric motors. 3: Reduction in power factor which is accompanied with more KVA demand. If there is a delta or grounded-star connection, the zero sequence current is eliminated. However, if there is no such connection, both zero and negative sequence current exist in the lines.

In these cases, the control performance of Voltage Source Inverter (VSI) would be influenced, leading to deteriorative power quality of microgrid. Therefore, it is necessary to develop the similar strategy to improve the power quality for microgrid in unbalanced conditions. Therefore, we need to have a controller that can share unbalanced current between all or part of sources in islanded microgrids[13].

A microgrid must be able to keep working under the unbalanced condition without any performance degradation, while the voltage unbalanced factor (VUF) should be held less than 2 percent for sensitive loads [14]. Therefore, the unbalanced current sharing strategy should consider this fact and do not let voltage unbalance increases from the threshold in any part of islanded microgrid.

The first step in a proper power sharing is to control the voltage and frequency [15] effectively. Several studies are conducted on unbalanced control strategy with second PI controllers to suppress the negative sequence components for an inverter with unbalance load[16,17], in which the voltages and currents are transferred by symmetry transformation firstly, and then the positive sequence and the negative sequence components are controlled by different PI controllers. However, the compensation strategy is applied to the individual operating inverter. Besides Proportional-integral (PI), The predictive deadbeat (DB), and proportional-resonant (PR) control technics are among the existing DG control methods. The PR controller is more efficient for the compensation of multiple harmonics due to the inclusion of nonlinear and unbalanced loads [18,19]. The next step toward uneven current sharing is managing fundamental power components, i.e., Active and Reactive power.

Active and reactive power sharing on Islanded microgrids control divides into two main strategies. The first method consists of strategies with communication in which each distributed generation unit sends data to a center, and the center decides for each unit to how much power each unit should produce. Another communication method is master-slave in which the master unit defines the voltage and frequency for the slave unit. The problem with the communication-based unit is that it needs transmission lines. Therefore, if the connection line is lost, the power management is interrupted [20]. Another problem with the communication-based method is that by adding a new source to the system, the whole system should be scheduled again. The other control method of microgrids are methods without communication.

One of the most important types of the control method in this class is droop method which is inspired by the behavior synchronous method. One of the main advantages of droop controller is its plug-and-play specification. It means that adding new sources doesn't need new scheduling so this method is more reliable than communication-based methods. In this paper, we use droop method

to share main power component such as active and reactive power. [21] proposes a new dynamic droop controller with the integration of SEMS/battery hybrid design to have a more stable frequency response in the Islanded microgrid while the battery lifetime increases. [22] proposes adaptive droop control with local measurement instrument to achieve genuine power sharing while reducing losses in the microgrid.

[20] propose a method to optimize droop coefficient to minimize the overall operation cost of islanded microgrid. In [23], the aim is to reduce frequency deviation in droop-based islanded microgrid with a mixed-integer linear programming method. In [24] a phase-angle droop control scheme is proposed to decrease system vulnerability in a severe situation such as storms or other natural disasters.

The conventional droop method is just based on proportional terms. To improve the speed response and accuracy of droop method, derivative and integral terms can be added to the droop [25,26]. Conventional droop is inspired by the ordinary network with rotating synchronous machine where the rotating inertia is coupled with the network, e.g., the inertia of synchronous machines. Therefore, the P/f droop control is dependent on the kinetic energy of the synchronous machine inertia. In an electronically interfaced microgrid, generally, less inertia is available. In larger microgrids, e.g., medium voltage microgrids, there is enough inertia thorough inductive line and larger scale of microgrids to connect P to the phase angle through frequency. However, in small-scale microgrids which usually are Low Voltage microgrids, this linkage is not strong enough since there is not enough inductance in the network and Microgrids are mostly resistive [27]. Therefore, the active power/ Voltage and reactive power/ frequency are becoming more popular in Low Voltage networks [28].

In conventional droop, since the voltage is not the same in all the network, the accuracy of reactive power sharing degrades [29]. Conversely, in P/V and Q/f droop, the accuracy of active power sharing degrades. There is a trade-off between the accuracy of active power sharing and droop parameters (deviation from the normal frequency and voltage value parameters). I.e., if the droop slopes are higher, the accuracy of active power sharing for P/V droop improves more. However, the voltage and frequency of the system will fluctuate more if a load is added or dropped. However, if the droop slopes are too low, the voltage and frequency deviation decrease but also it affects active power sharing negatively [30,31]. Although droop method is a practical way to share the main component of power such as active and reactive, it is unable to share another power component such as harmonic and unbalanced current in islanded microgrids.

To solve the unbalanced problem [32,33] suggested control method and strategies. [32], first investigate the relationship between active and reactive power oscillation in the presence of an unbalanced load and propose a plan to suppress the power oscillation that is caused by the unbalanced load.

[33] offers a new strategy for unbalance and nonlinear load in islanded microgrid. One of the sources is responsible for supplying unbalanced and nonlinear current while other sources just share active and reactive power. The problem with this strategy is when unbalance load is far from the dedicated source, severe unbalance voltage will happen in the microgrid.

A plan for the scheduling of unbalanced microgrids is proposed in[34] build on the method of a multi-objective optimization problem, whose objective functions are related to specific services and requirements of the microgrid, such as cost minimization, power quality improvements, and energy savings. [23] employs adaptive Lyapunov function based control scheme to compensate the negative sequence current in some part of microgrid and by applying sliding mode based control scheme, regulate positive-sequence active and reactive power in the microgrid. One way of compensating unbalance current is using Active Power filters (APF)[35,36]. In this method, the negative sequence voltage, current is added to the series and shunt APF respectively. To compensate unbalance voltage, the[35] propose using two inverter structure. The first one connects as a shunt and the other connected as a series AFP. [37] uses model predictive control (MPC) technique to minimize the voltage unbalance.

138 The MPC is combined with the V-I droop to provide a fast dynamic response. The concept of using
139 virtual impedance becomes more and more prevalent in the control system of microgrids.

140   The first attempt to use virtual impedance concept return to [38] When virtual impedance was
141 used to control a DC-DC converter. The use of virtual impedance is becoming more and more common
142 in the case of controlling power electronic based instruments. One of the main application of virtual
143 impedance is to help improve power sharing [39,40]. In microgrids the ratio of x/r is low. Therefore, the
144 accuracy of reactive power sharing decreases. By adding an inductive virtual impedance to the control
145 loop, the accuracy of reactive load sharing improves significantly [39,41,42]. The virtual impedance is
146 used to improve stability robustness against different scenarios in microgrid such as severe transient
147 and fault situations[43,44]. Another use of virtual impedance is to promote load sharing among parallel
148 converters[45–47]. in[48,49] adaptive virtual impedance is introduced to enhance power distribution
149 further regardless of line impedance unbalances, linear and nonlinear loads.

150   It can be used to reduce harmonic/unbalanced current or voltage on the converters [50]. In [51,52],
151 the negative-sequence voltage produced by negative-sequence impedance controller loop is injected
152 directly to the reference signal of the voltage controller. The idea is to change negative-sequence
153 impedance of each unit so that the amount of negative-sequence current of each DG is controlled. In
154 [53], the above idea of using virtual negative-sequence impedance is used, but the negative-sequence
155 voltage produced by the loop is directly injected to the control signal of the inverter.

156   To the best of our knowledge, the virtual impedance method has not been used for controlling the
157 zero-sequence current in LV microgrids. In this paper, the virtual zero-sequence impedance together
158 with the virtual negative-sequence impedance are used to control the zero- and negative-sequence
159 currents in an LV microgrid. The proposed strategy relies on the fact that the adjacent DG of an
160 unbalanced load should compensate the negative- and zero-sequence currents of that load. Moreover,
161 if the negative- and zero-sequence currents of the load exceeds the maximum capacity of its own
162 DGs, the remaining portion of the negative- and zero-sequence currents are shared among other DGs.
163 Although there are numerous method in the literature about unbalance compensation, few of the
164 focus on islanded microgrids. Table 1 shows summary of converter interfaced method that deals with
165 unbalance problem. Most of the method is related to keeping the unbalanced voltage of the terminal
166 of a single inverter or UPS below a limit by providing enough unbalanced current for the load.

167   These control methods are not concerned about power-sharing and other power components
168 since there is only one unit. Although these methods are effective to keep unbalanced voltage control,
169 the effectiveness of them is not evaluated. Another group of research deals with the parallel inverters
170 while feeding the loads connected to a common line. The control method in this group is more complex
171 than the previous method.

172   The control strategy should not only be able to control voltage and frequency of each unit; they
173 should be able to control circulating negative sequence current flowing in the system. Since the system
174 is usually Three-wired, the zero sequence current is not a concern. The third group of methods deals
175 with the grid-connected MG. the frequency and voltage are dictated by the main grid. Therefore, these
176 control methods are in charge of active and reactive power and also other power components such
177 as harmonic and unbalanced currents. also , if the MG cannot provide enough unbalanced current,
178 the main grid can compensate for it. The fourth group is the islanded-microgrids. The most complex
179 control method belongs to this group. It control method not only should be able to control voltage and
180 frequency by itself, but it should also be able to control and active and reactive power components
181 and harmonic and unbalanced current altogether. One type if MG is low voltage ones. since they are
182 three-phase four-wired, zero sequences can flow in the network alongside negative and positive one
183 when an unbalanced load is present in the network. From the very few papers that specifically focused
184 on unbalanced current sharing, almost all of them focused on negative sequence current sharing and
185 zero sequence current sharing is not addressed except only just one work.

Table 1. Method Comparison.

Focus	Main Duties	Unbalanced Current Sharing Duties	Unbalancy Challange		
			Unbalanced Voltage Control	Negative Sequence Sharing	Negative and Zero Sequence Sharing
UPS and single Inverter	Voltage, frequency	current sharing is not a problem since there is only one unit to provide the current	[33,35]	✗	✗
Parallel Inverter	Voltage, frequency, circulating current	the main challenge is to stop circulating unbalanced current between units	[41,42,45,54]	[41,42,54]	[45]
Grid-Connected MG	sharing active and reactive power	keeping unbalanced voltage under control.if MG can not provide enough unbalanced current, the main grid can provide the rest	[23,32,34]	[23,32,34]	Non
Islanded MG	voltage, frecuency, sharing active and reactive power	keeping unbalanced voltage under control while unbalanced current is shared only between DG units since there is no main grid to provide remaining unbalanced currents	[47,49,52,53,55]	[47,49,52,53, 55]	Non

2. Methods

some introductory text

2.1. Multi-bus low voltage microgrid structure

Fig. 1(a) shows a single-line diagram of a multi-bus LV microgrid that consists of three LV feeders and two electronically-coupled three-phase four-wire DG units. Loads in the three radial feeders can be either balanced or unbalanced. The DG units connected via feeders $F1$ and $F2$ to the microgrid are assumed to be dispatchable. Therefore, they can provide any amount of real/reactive power within their pre-specified limits. Each unit has to maintain its voltage and frequency in the pre-specified level, while an accurate power-sharing is ensured through a decentralized method. The loads are connected to the microgrid through four wires. Therefore, the load current can have zero-sequence current in addition to the negative-sequence current when loads in the microgrid are unbalanced. In this paper, it is assumed that microgrid works in islanded mode of operation. Therefore, the microgrid is responsible for compensating zero- and negative-sequence currents of unbalanced loads. If the
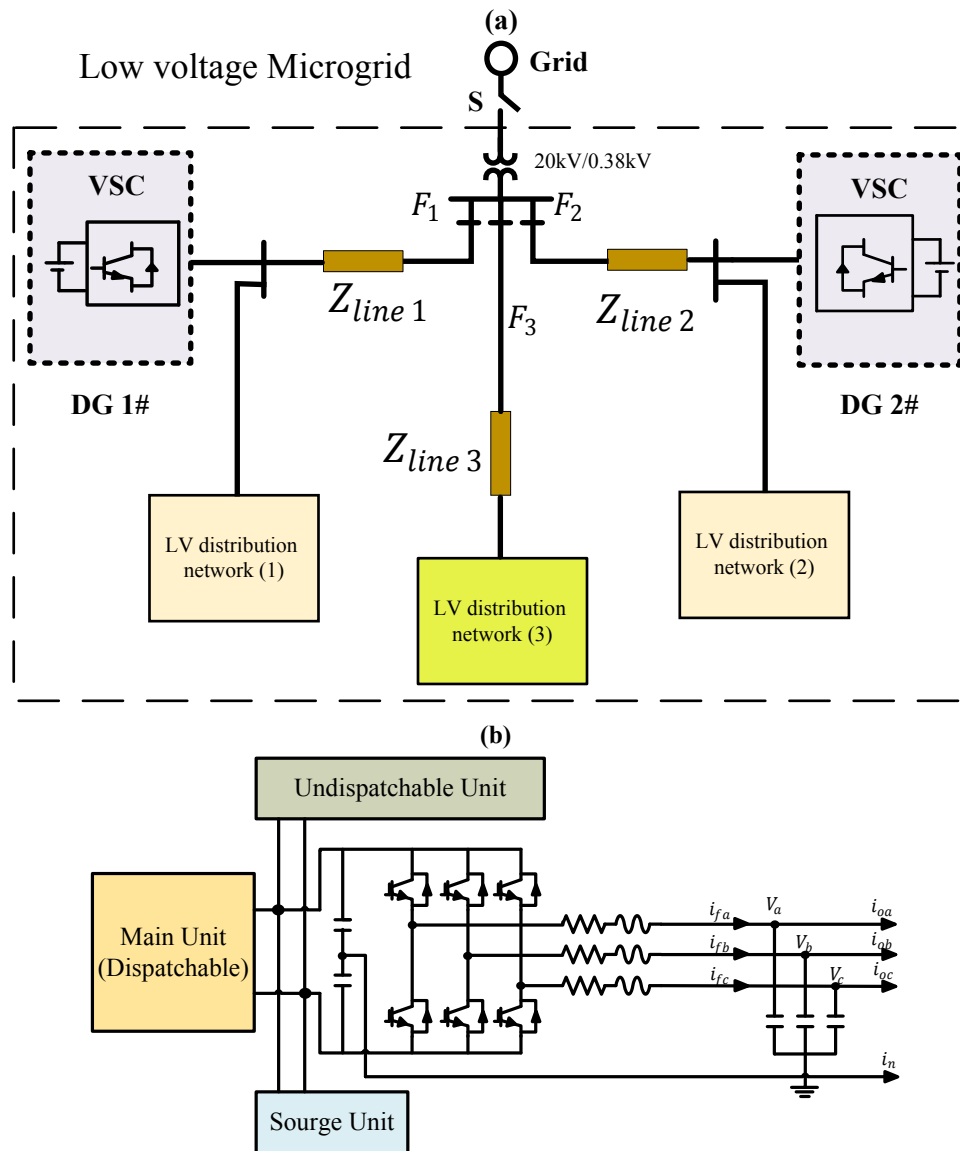
Figure 1. (a) LV multi-bus MG consisting of two DG units and (b) three-phase four-wired inverter.

islanded microgrid does not compensate these currents, the voltage will be distorted. Table 3 shows the microgrid parameters.

Each DG unit with its *LC* filter is considered as a subsystem for the microgrid. In order to control each DG unit, the first step is to drive the dynamic model of each DG unit. Fig. 2 shows an equivalent circuit diagram of a three-phase four-wire DG subsystem. The objective is to design a feedback control that robustly regulates the load voltages while the load current is unknown. In [53], dynamic model for a three-phase three-wired network in the stationary reference frame ($\alpha\beta$) is derived. Because this microgrid is a four-wire system, three separate state-space parameters are required to control the microgrid voltage.

$$\dot{\mathbf{X}} = \mathbf{AX} + \mathbf{BU} + \mathbf{EW}$$
$$\mathbf{Y} = \mathbf{CX} \tag{1}$$
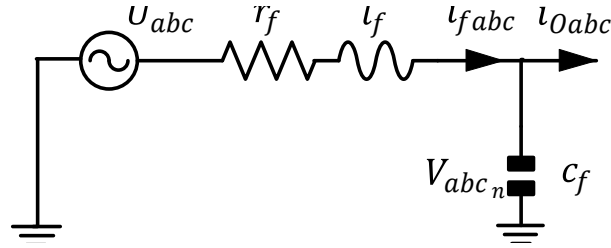
Figure 2. Single phase diagram of inverter.

where $\mathbf{X} = \begin{bmatrix} v_\alpha, v_\beta, v_0, i_{f_\alpha}, i_{f_\beta}, i_{f_0} \end{bmatrix}^T$, $\mathbf{U} = \begin{bmatrix} U_\alpha, U_\beta, U_0 \end{bmatrix}^T$, $\mathbf{W} = \begin{bmatrix} i_{o\alpha}, i_{o\beta}, i_{o_0} \end{bmatrix}^T$, $\mathbf{Y} = \begin{bmatrix} v_\alpha, v_\beta, v_0 \end{bmatrix}^T$ and

$$
\mathbf{A} = \begin{bmatrix}
0 & 0 & 0 & \frac{1}{C_f} & 0 & 0 \\
0 & 0 & 0 & 0 & \frac{1}{C_f} & 0 \\
0 & 0 & 0 & 0 & 0 & \frac{1}{C_f} \\
-\frac{1}{L_f} & 0 & 0 & -\frac{r_f}{L_f} & 0 & 0 \\
0 & -\frac{1}{L_f} & 0 & 0 & -\frac{r_f}{L_f} & 0 \\
0 & 0 & -\frac{1}{L_f} & 0 & 0 & -\frac{r_f}{L_f}
\end{bmatrix}
$$

$$
\mathbf{B} = \begin{bmatrix}
0 & 0 & 0 \\
0 & 0 & 0 \\
0 & 0 & 0 \\
\frac{1}{L_f} & 0 & 0 \\
0 & \frac{1}{L_f} & 0 \\
0 & 0 & \frac{1}{L_f}
\end{bmatrix} \quad
\mathbf{E} = \begin{bmatrix}
-\frac{1}{C_f} & 0 & 0 \\
0 & -\frac{1}{C_f} & 0 \\
0 & 0 & -\frac{1}{C_f} \\
0 & 0 & 0 \\
0 & 0 & 0 \\
0 & 0 & 0
\end{bmatrix}
$$

$$
\mathbf{C} = \begin{bmatrix} 1 & 0 & 0 & 0 \\ 0 & 1 & 0 & 0 \end{bmatrix}.
$$

(2)

The transfer function representation of equation (1) is obtained as:

$$
V_{\alpha\beta0}(s) = G_{(3\times3)}(s)U_{\alpha\beta0}(s) - Z_{(3\times3)}(s)I_{o\alpha\beta0}(s)
$$

(3)

where $G_{(3\times3)}$ and $Z_{(3\times3)}(s)$ are:

$$
g_{12}(s) = g_{13}(s) = g_{21}(s) = g_{23}(s) = g_{31}(s) = g_{32}(s) =
$$
$$
z_{12}(s) = z_{21}(s) = z_{21}(s) = z_{23} = (s)z_{31}(s) = z_{32}(s) = 0
$$
$$
g_{11}(s) = g_{22}(s) = g_{33}(s) = \frac{1}{L_f C_f s^2 + r_f C_f s + 1}
$$
$$
z_{11}(s) = z_{22}(s) = z_{33}(s) = \frac{L_f s + r_f}{L_f C_f s^2 + r_f C_f s + 1}.
$$

(4)

Equation (4) shows that the matrix transfer function of each DG control system is diagonal (completely decoupled) and can be regarded as three SISO control systems. Therefore, the problem of designing a three-inputs three-outputs control system, is reduced to design three one-input one-output systems.

2.2. Operation Principles of the Proposed Control Strategy

The single line diagram of the LV microgrid that is studied in this paper is shown in Fig. 1(a). The RMS of the phase-to-ground output voltage of DGs in this network is 220 V. All DG units are interfaced to the microgrid through DC/AC converters. The dc-side of each inverter is equipped with multiple sources which consist of a dispatchable unit, such as micro-turbine, a non-dispatchable unit such as the photovoltaic cell, and a surge unit which supplies the system in severe transient conditions. Therefore, these three units provide almost a constant DC voltage for the inverter [56]. Therefore, the energy source of each DG unit is modeled by an ideal dc voltage source, and the dynamics of DC part of the inverter is not considered in this study.
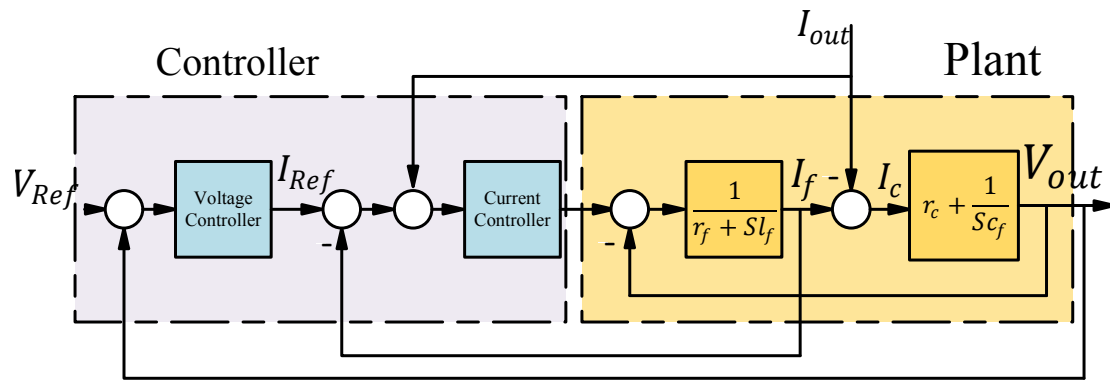
Figure 3. plant for voltage and current controller.
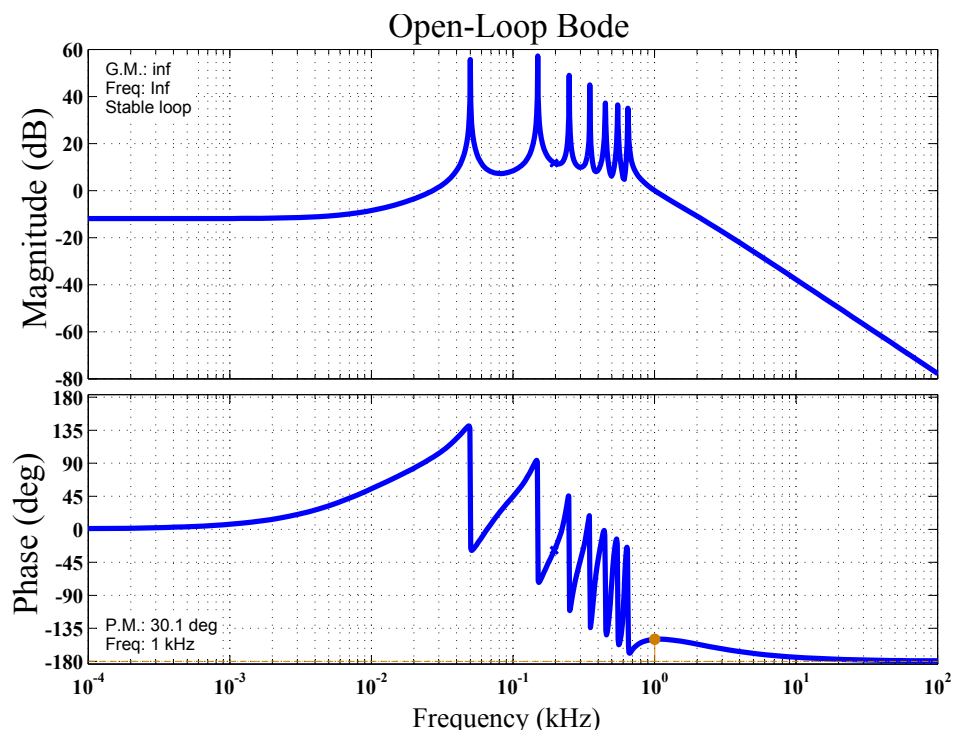
Figure 4. Bode diagram.
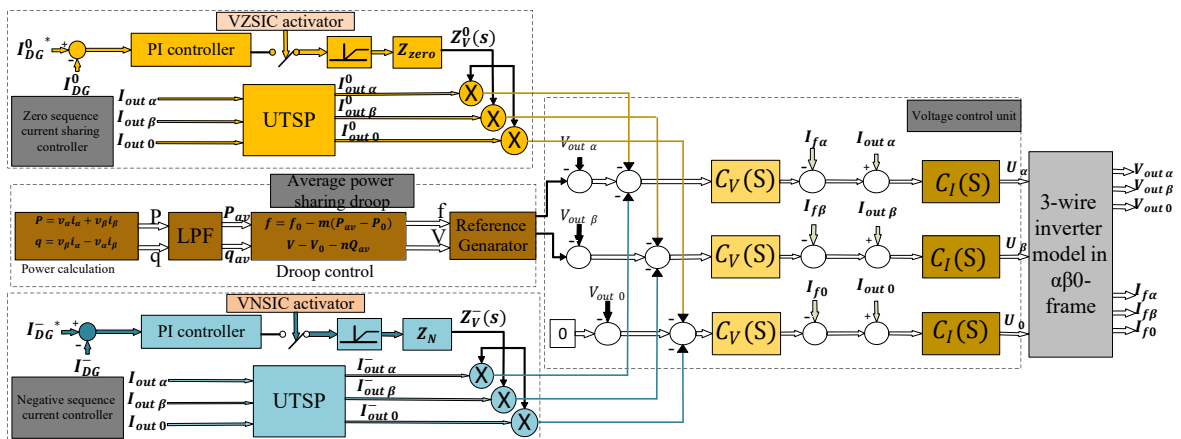
Figure 5. Control unit of DG units.

Table 2. Controllers parameters.

Parameter	C_I	C_V
$C(s)$	-	$g_c = 3.7, z = 60, p = 8e^3$
K_p	1	17.71
K_{I_1}	600	$5e^3$
K_{I_3}	$1e^3$	$7e^3$
K_{I_5}	$1.2e^3$	$4.5e^3$
K_{I_7}	$1.6e^3$	$5e^3$
K_{I_9}	$2.6e^3$	$10e^3$
$K_{I_{11}}$	$2.8e^3$	$14e^3$
$K_{I_{13}}$	-	$17e^3$
ω_0	$2 \times 50 \times \pi$	$2 \times 50 \times \pi$
ω_c	π	π

222   Controllers are designed in the stationary reference frame ($\alpha\beta 0$) which is presented in [53]. It is
223   noted that designing controllers is easier in the synchronous reference frame ($dq0$) than the stationary
224   reference frame ($\alpha\beta 0$). However, it should be noted that these controllers cannot effectively control a
225   microgrid with unbalanced loads. The proposed control strategy of each unit consists of; 1) current
226   controller; 2) voltage controller; 3) average power sharing controller, and 4) negative- and zero-sequence
227   currents controller. The current and voltage controllers are proportional resonance (PR) controllers.
228   In islanded microgrid, it is not necessary to use PR controller as the current controller since using a
229   simple proportional controller would suffice. However, by using a PR controller as current controller,
230   the proposed control strategy can be used both in islanded mode and grid-connected mode. Therefore,
231   using this controller as the current controller can reduce the cost of design and operation of DG units,
232   while the microgrid can smoothly switch between islanded and grid-connected modes.

233   Under unbalanced load condition, the instantaneous power has a double-frequency oscillatory
234   term in addition to the DC power [57]. The conventional droop controller which is widely adopted
235   to share average power component is not able to share the oscillatory power component among the
236   DG units. In [51,58], a virtual negative-sequence impedance controller (VNSIC) was proposed to
237   share the negative-sequence current. However, this approach has not been adopted for zero-sequence
238   current sharing. In this paper, the same approach is adopted to share the zero-sequence current. By
239   controlling the flow of negative- and zero-sequence currents of each DG unit, oscillatory part of the
240   power of each unit is shared according to its capacity. The strategy for the compensation of zero- and
241   negative-sequence currents is based on the compensating unbalanced loads by its upstream DG unit.
242   Moreover, for loads with no upstream DG unit, the negative- and zero-sequence currents are shared
243   by adjacent DG units. By deploying this strategy, the flow of negative- and zero-sequence currents in
244   microgrid is minimized, and DG units compensate these currents according to their capacity. Hence,
245   the overall power quality of the the microgrid is improved.

2.3. Proportional Resonance Controller

247   Because the matrix transfer function of the DG subsystem in (4) is diagonal, the three identical
248   SISO controllers can be independently designed for the quadrature axes α, β and 0. Fig. 3 shows the
249   structure of the voltage and current controllers for the α, β and 0 axes. A good controller should be
250   able to track the reference signal with minimum transient and error while it should guarantee a low
251   THD of voltage in the presence of harmonic loads. Since the controllers are designed in the stationary
252   framework, reference signals are sinusoidal. Therefore, the multi-proportional-resonant controller
253   (MPRC) is used. MPRC can track sinusoidal references with zero tracking error, while conventional PI
254   controller has magnitude and phase error and can not effectively track sinusoidal signals. Therefore,
255   MPRC can handle harmonic loads without deteriorating voltage quality. By using MPRC as the current
256   controller, the control structure can be used in the grid-connected mode of operation as well. Therefore,
257   there is no need for a different control structure in grid-connected mode. As a result, the total cost

²⁵⁸ for design and operation of microgrid decreases. Matlab SISO Tool software is used to design the
²⁵⁹ controllers. The transfer function of MPRC is as follows:

$$C_V \ and \ C_I : C(s)[K_p + \Sigma K_{i_h} \frac{s}{s^2 + 2h\omega_c s + (h\omega_0)^2}],$$

$$C(s) = g_c \frac{s+z}{s+p} \tag{5}$$

²⁶⁰   Where $C(s)$ is a lead compensator that is added to the structure of the voltage controller to increase
²⁶¹ the phase margin and bandwidth of the system. Fig. 4 shows the Bode diagram of the voltage control
²⁶² loop system. As it is seen from this figure, the system has a good gain margin and a phase margin
²⁶³ of 30 degrees while the bandwidth is about 1 kHz. Therefore, the controller shows a robust stability
²⁶⁴ margin, and very fast response to load step changes. It also provides and excellent noise and harmonic
²⁶⁵ rejection capability due to its high bandwidth. The coefficients of current and voltage controllers are
²⁶⁶ given in Table 2.

²⁶⁷ *2.4. Proposed Control System*

²⁶⁸   Fig. 5 shows the block diagram of the proposed control system. The voltage controller consists
²⁶⁹ of three identical MPRC whose reference signals are determined by the droop control strategy. The
²⁷⁰ droop coefficients, i.e., *m*, *n* are obtained according to the rated power of each DG and the maximum
²⁷¹ deviation of frequency and voltage [59]. The instantaneous real power is calculated using output
²⁷² current and voltage of each DG based on the instantaneous power theory that is proposed in [57].
²⁷³ The instantaneous power is passed through a low pass filter to attenuate the ripples that are caused
²⁷⁴ by unbalanced and harmonic loads. The average power is then applied to the droop controller to
²⁷⁵ determine the working frequency and the voltage magnitude of each DG unit. Then, the voltage
²⁷⁶ and frequency are applied to the reference generator to produce a symmetrical three-phase reference
²⁷⁷ voltage. Since the control structure is in the stationary frame, the Clark transformation is applied to the
²⁷⁸ symmetrical voltage. Therefore, the zero parameters of the Clark transformation will always be zero
²⁷⁹ since the reference voltage is always symmetrical. The output of voltage controller is the reference for
²⁸⁰ the current controller and is compared with the current of the filter inductance. The resultant current
²⁸¹ is then feedforwarded to the output current which improves the system stability. The output of the
²⁸² current controller is then applied to the inverter.
²⁸³   To control the zero- and negative-sequence currents, zero- and negative-sequence current
²⁸⁴ controllers are used, respectively. In these blocks, the output current of each DG unit ($I_{\alpha\beta 0}$) is
²⁸⁵ decomposed to its symmetrical component with a unified three-phase signal processor (UTSP) [60]. The
²⁸⁶ UTSP block can accurately decompose the symmetrical parameters of current, so that, the instantaneous
²⁸⁷ amount of zero- and negative-sequence currents can be obtained from the output current.
²⁸⁸   The extracted zero- and negative-sequence currents are multiplied by a resistive or inductive
²⁸⁹ impedance gain, Z_V^- and Z_V^0 respectively to produce the references for zero- and negative-sequence
²⁹⁰ voltages. These voltages are then added to the reference signals of the voltage controller. The values of
²⁹¹ Z_V^- and Z_V^0 are determined by the virtual negative-sequence impedance controller (VNSIC) and the
²⁹² virtual zero-sequence impedance controller (VZSIC). The virtual impedance blocks compare negative-
²⁹³ and zero-sequences of each unit with its negative- or zero-sequence references. The resultant signal
²⁹⁴ is then passed through a PI controller and then multiplied by a resistive or inductive impedance to
²⁹⁵ generate the reference for the virtual impedance of zero- or negative-sequence impedances of each DG
²⁹⁶ unit.

²⁹⁷ 2.4.1. Positive-, Negative- and zero-sequence Models of DG Units

   To accurately control a DG unit, the dynamic model of Fig. 5 can be divided into positive-,
negative- and zero-sequence elements. In [58], dynamic model of the system is divided into positive

and negative elements. The same procedure can be adopted to extract the zero-sequence dynamic model. In Fig. 5, the voltage of the closed-loop system in the $\alpha\beta0$-frame can be expressed as:

$$
\begin{aligned}
V_{\alpha,\beta,0}(s) = H(s)[V^*_{\alpha,\beta,0}(s) - Z^-_V(s)I^-_{o_{\alpha,\beta,0}}(s) \\
- Z^0_V(s)I^0_{o_{\alpha,\beta,0}}(s)] - Z_{out}(s)I_{o_{\alpha,\beta,0}}(s)
\end{aligned}
\tag{6}
$$

where $V_{\alpha,\beta,0}$ and $I_{o_{\alpha,\beta,0}}$ are the voltage reference signal and the DG terminal current, respectively. $H(s)$ denotes the closed-loop transfer function from the reference signal to the output voltage, while $Z_{out}(s)$ is the output impedance. $I^-_{o_{\alpha,\beta,0}}$ and $I^0_{o_{\alpha,\beta,0}}$ are the instantaneous negative and zero-sequence components of $I_{o_{\alpha,\beta,0}}$. $Z^-_V(s)$ and $Z^0_V(s)$ are the virtual impedances that are determined by the VNSIC and the VZSIC, respectively. The virtual impedance can be inductive or resistive or a combination of both [58]. Equation (6) can be rewritten as:

$$
\begin{aligned}
V^+_{\alpha,\beta0}(s) + V^-_{\alpha,\beta,0}(s) + V^0_{\alpha,\beta,0}(s) = H(s)V^*_{\alpha,\beta,0}(s) \\
- Z_{out}(s)I^+_{o_{\alpha,\beta,0}}(s) - [Z^-_V(s)H(s) + Z_{out}(s)]I^-_{o_{\alpha,\beta}}(s) \\
- [Z^0_V(s)H(s) + Z_{out}(s)]I^0_{o_{\alpha,\beta,0}}(s).
\end{aligned}
\tag{7}
$$

Equation (7) can be divided into positive- , negative- and zero-sequence voltages. Therefore, the output voltage of DG unit can be expressed as:

$$
\begin{cases}
V^+_{\alpha,\beta,0}(s) = H(s)V^*_{\alpha,\beta,0}(s) - Z_{out}(s)I^+_{o_{\alpha,\beta,0}}(s) \\
V^-_{\alpha,\beta,0}(s) = -[Z^-_V(s)H(s) + Z_{out}(s)]I^-_{o_{\alpha,\beta,0}}(s). \\
V^0_{\alpha,\beta,0}(s) = -[Z^0_V(s)H(s) + Z_{out}(s)]I^0_{o_{\alpha,\beta,0}}(s).
\end{cases}
\tag{8}
$$

298   In the working condition of microgrid $H(\vec{j}\omega_0) = 1\angle 0$. In this paper the virtual impedances Z^-_V
299 and Z^0_V are chosen to be inductive. Therefore, the negative-sequence impedance of each DG unit at the
300 system frequency is:

$$
\begin{aligned}
Z^-_{out}(j\omega_0) = Z^-_V(j\omega_0) + Z_{out}(j\omega_0) \\
= R_{out}(\omega_0) + j[X_{out}(\omega_0) + X^-_V(\omega_0)]
\end{aligned}
\tag{9}
$$

301 Moreover, the zero-sequence impedance at the system frequency is:

$$
\begin{aligned}
Z^0_{out}(j\omega_0) = Z^-_V(j\omega_0) + Z_{out}(j\omega_0) \\
= R_{out}(\omega_0) + j[X_{out}(\omega_0) + X^0_V(\omega_0)]
\end{aligned}
\tag{10}
$$

302   To control the negative- and zero-sequence voltages that are injected to the reference of the voltage
303 controller, the X^-_V and X^0_V can be changed. The values of these parameters are set by the VNSIC and
304 the VZSIC of each unit. The negative- and zero-sequence voltages are then injected to the reference of
305 the voltage controller. Therefore, by controlling the negative- and zero-sequence voltages of each unit,
306 the negative- and zero-sequence output currents of each unit are controlled. The maximum permissible
307 values for $X^-_V(\omega_0)$ and $X^-_V(\omega_0)$ can be calculated based on the IEEE standards [14,61]. Negative- and
308 zero-sequence unbalanced factors are equal to:
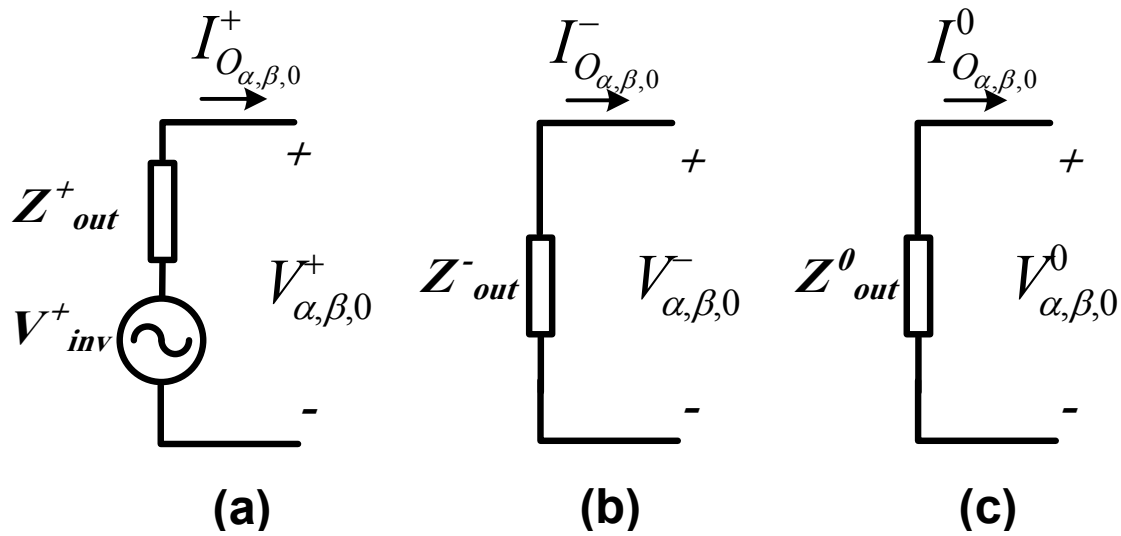
Figure 6. (a) Positive-, (b) negative- and (c)zero-sequence models of the DG unit.

$$(VUF)^- = \frac{V^-_{\alpha,\beta,0}}{V^+_{\alpha,\beta,0}} = \frac{Z^-_{out}I^-_{o_{\alpha,\beta,0}}}{V^+_{\alpha,\beta,0}} < 0.02$$

$$(VUF)^0 = \frac{V^0_{\alpha,\beta,0}}{V^+_{\alpha,\beta,0}} = \frac{Z^0_{out}I^0_{o_{\alpha,\beta,0}}}{V^+_{\alpha,\beta,0}} < 0.02 \tag{11}$$

309   Another limiting factor associated with the injection of the negative- and zero-sequence currents
310 is the capability of each unit to inject these currents. Therefore, the capacity of each unit and the
311 inequality constraint in(11) determine the maximum value of the negative- and zero-sequence output
312 impedances. Based on (8), the positive-, negative-, and zero-sequence models for each DG unit are
313 obtained and is shown in Fig. 6.

314 2.4.2. Negative- and zero-sequence Currents Sharing Strategy

315   In the previous Section, the technical procedure for controlling negative- and zero-sequence
316 currents was explained. In this Section, the zero- and negative-sequence current sharing strategy
317 is proposed so that it minimizes the flow of the unbalanced current throughout the LV microgrid.
318 Therefore, the overall power quality of microgrid improves. With the use of an accurate power-sharing
319 strategy, not only the overall power quality of microgrid is improved, but also the proper autonomous
320 operation of the microgrid is guaranteed. In this strategy, the unbalanced current of each load is
321 compensated by its upstream unit. However, the unbalanced currents of loads with no upstream unit
322 are shared by its adjacent units. Considering these two conditions, the reference for negative- and
323 zero-sequence currents of each unit must be as follows:

$$I_{DG}^{-}{}^{*} = \sqrt{I_{loc}^{-}{}^{2} + I_{nonloc}^{-}{}^{*2} + 2I_{loc}^{-}I_{nonloc}^{-}{}^{*}\cos\theta_{-}}$$

$$I_{DG}^{0}{}^{*} = \sqrt{I_{loc}^{0}{}^{2} + I_{nonloc}^{0}{}^{*2} + 2I_{loc}^{0}I_{nonloc}^{0}{}^{*}\cos\theta_{0}} \tag{12}$$

324 Where I_{loc}^{-} and I_{loc}^{0} are magnitudes of the negative- and zero-sequence currents of the local loads,
325 respectively. θ_{-} and θ_{0} are the phase difference between I_{loc} and I_{nonloc}^{*} for the negative- and
326 zero-sequence currents, respectively.

$I_{nonloc}^{-}{}^{*}$ and $I_{nonloc}^{0}{}^{*}$ are defined as:

$$I_{nonloc}^{-}{}^{*} = \frac{I_{max_{DGi}}^{-}}{\sum I_{max_{DGi}}^{-}} I_{nonloc}^{-}, I_{nonloc}^{0}{}^{*} = \frac{I_{max_{DGi}}^{0}}{\sum I_{max_{DGi}}^{0}} I_{nonloc}^{0} \qquad (13)$$

In (13), $I_{max_{DGi}}^{-}$ and $I_{max_{DGi}}^{0}$ are respectively the maximum negative- and zero-sequence currents that the ith DG can inject. I_{nonloc}^{-} and I_{nonloc}^{0} are the amplitudes of the negative- and zero-sequence of feeders supplying the nonlocal load. Referring to (13) and (12), the local unbalanced loads are compensated locally while the unbalanced loads with no upstream DG unit are shared among all DG units according to their unbalanced load capacity. By using PMU[1] which is installed on feeders, the phase difference between local and nonlocal currents is calculated. If all impedances of lines are known, the PMU unit can be omitted. Since the impedances of lines are usually unknown, with the help of PMU unit, an accurate power sharing can be achieved. This method has an advantage over other power sharing method that only considers amplitude of unbalanced currents as it considers both amplitude and phasor of unbalanced currents. For example, in some scenarios, the unbalanced currents of some loads can nullify those of other loads, while the DG unit remains under balanced condition. So if the phasor of currents is not considered, the reference currents for virtual impedance loop will not be accurate. In the proposed control strategy, the VNSIC and VZSIC are enabled when: 1) The DG unit reaches to its maximum capacity so that it is not able to inject the required negative and zero sequence currents. When the VNSIC and the VZSIC are disabled, the virtual impedances of the unit are kept at the minimum value, i.e., $X_V^{-}=X_V^{0}=0$. This means that the DG unit compensates all unbalanced loads in its downstream. When a DG unit reaches to its maximum capacity, X_V^{-} and X_V^{0} are changed to prevent the unit from overloading. 2) The control system of the DG unit detects unbalanced current flow from adjacent feeders. Therefore, the DG units change their virtual impedances accordingly to share the remaining unbalanced currents. Otherwise, the VNSIC and VZSIC are disabled, and the negative- and zero-sequence of the output impedances are kept constant at the minimum value. When VNSIC and VZSIC are activated, the PI controllers set Z_V^{0} and Z_V^{-} to a desirable value.

3. Results and Discussion

To verify the effectiveness of the proposed control strategy, the LV microgrid showed in Fig. 1 (*a*) has been simulated in PSCAD/EMTDC environment. The LV microgrid is assumed to operate in islanded mode and comprises a three-feeder distribution system with two electronically-coupled four-wire dispatchable DG units. All DG units are equipped with the PR controller, droop control strategy, VNSIC, and VZSIC. The parameters of microgrid including all DG units are given in Tables 2 and 3. Several load changes are introduced to the microgrid aiming to verify its dynamic performance.

3.1. Case study I

In this case study, initially, two balanced loads are connected to feeders F_1 and F_3. The load that is connected to feeder F_3 is a three-phase *RL* load with the nominal power of 285 kVA and a power factor of *PF*=0.88, while the load connected to feeder F_1 is a three-phase *RL* load with 75 kVA with *PF*=0.9. A single-phase load rated 40 kVA with *PF*=0.98 is connected to one phase of feeder F_1 at *t*=2 s. Subsequent to this load change, at *t*=5 s, another single-phase load rated 26 kVA with *PF*=0.95 is connected to the same phase of feeder F_1. The instantaneous real and reactive powers considering these load changes are shown in Fig. 8. Since feeder F_1 becomes unbalanced, a double-frequency ripple appears on the instantaneous power components of this feeder. As it is observed, the double-frequency ripple amplitude increases as another unbalanced load is connected to the feeder F_1 at *t*=5 s. Fig. 9

---

[1]   phasor measurement unit

Table 3. MG system parameters.

Parameter	Value	Comments
S_{base}	300 kVA	DG ratings
Z_{line1}	0.04 + j 0.0157 $p.u.$	0.8 km overhead line
Z_{line2}	0.07 + j 0.0332 $p.u.$	1.3 km overhead line
Z_{line3}	0.01 + j 0.0022 $p.u.$	0.2 km overhead line
L_{f1}, L_{f2}	0.3 mH	series filter inductance
r_{f1}, r_{f2}	0.0015 Ω	series filter resistance
C_{f1}, C_{f2}	2200 μF	filter capacitance
V_{dc}	1500 V	dc bus voltage
f_s	6 kHz	switching frequency
$P_{DG_1}, 2, P_{DG_2}$	100 KW	maximum real power
Q_{DG_1}, Q_{DG_2}	100 kVAr	maximum reactive power
m_{DG_1}, m_{DG_2}	3.33 Hz/MW	P-f droop coefficients
n_{DG_1}, n_{DG_2}	3.26V/MVAr	Q-V droop coefficients
$I^-_{max_{DG_1}}, I^-_{max_{DG_2}}$	97 A (0.13 p.u.)	
$I^0_{max_{DG_1}}, I^0_{max_{DG_2}}$	97 A (0.13 p.u.)	
k_{Pn_1}, k_{In_1}	$3e^{-6}, 1e^3$	VNSIC parameters of DG_1
k_{Pn_2}, k_{In_2}	$3e^{-6}, 1e^3$	VNSIC parameters of DG_2
k_{Pz_1}, k_{Iz_1}	$1e^{-6}, 2e^3$	VZSIC parameters of DG_1
k_{Pz_2}, k_{Iz_2}	$1e^{-6}, 2e^3$	VZSIC parameters of DG_2
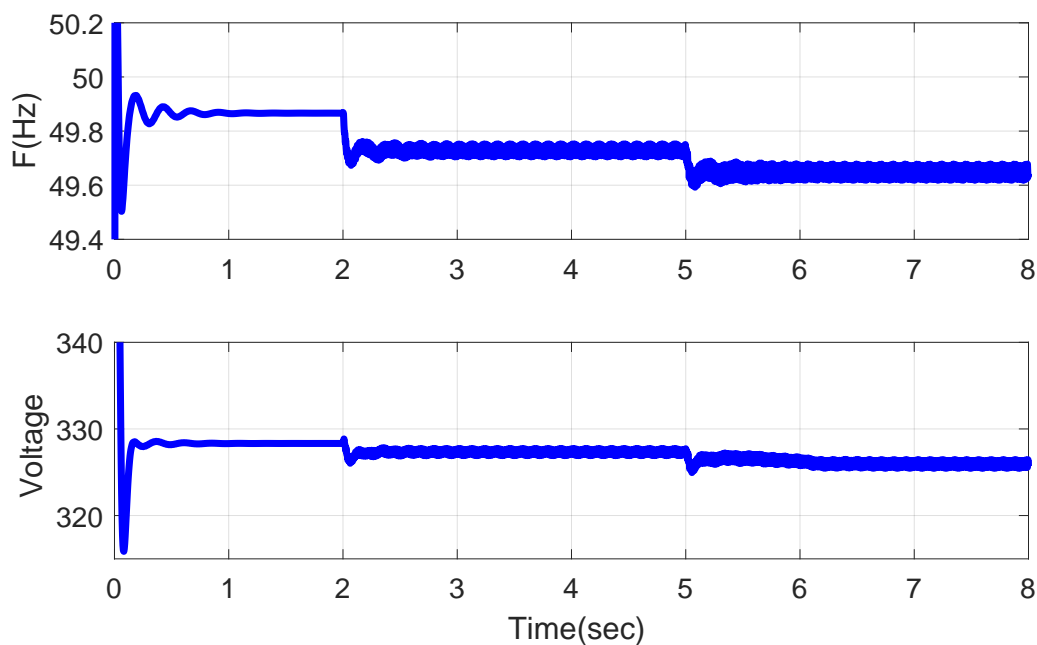
Figure 7. Instantaneous voltages at the DG terminals during unbalanced load changes in feeder F_1, (a) DG_1 and (b) DG_2.
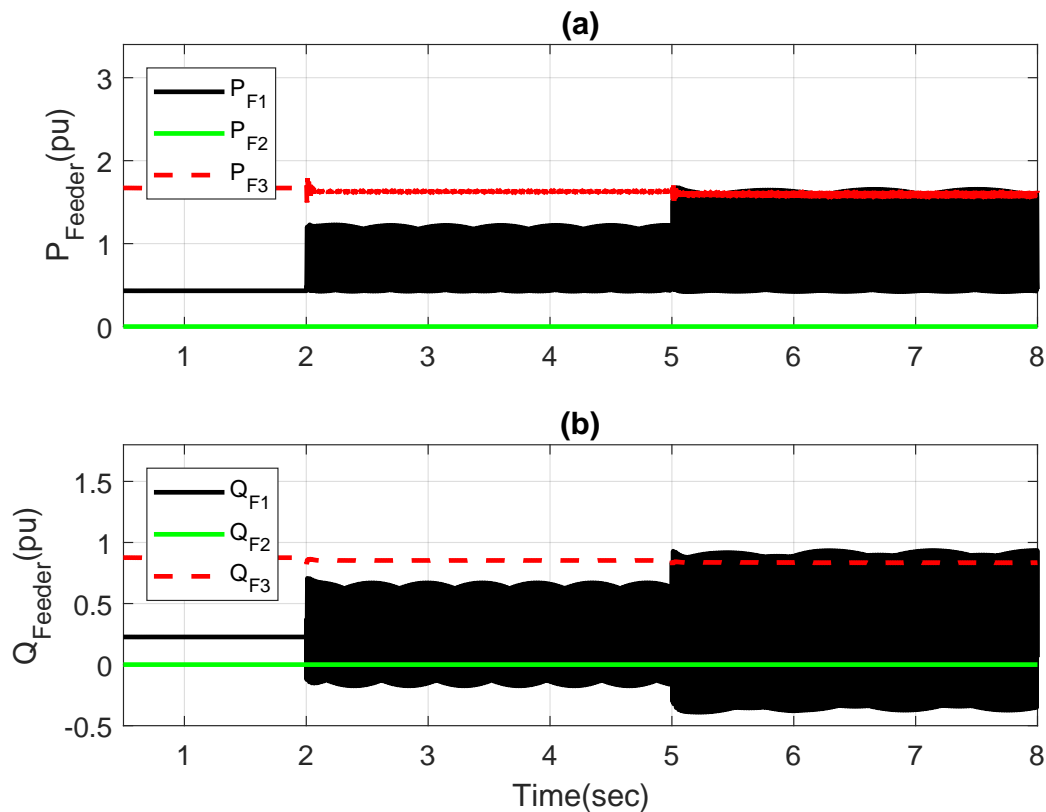
Figure 8. Unbalanced load changes in feeder F_1 (a) instantaneous real and (b) reactive power of feeders.

366   shows the positive-, negative- and zero-sequence current components of feeder F_1 that increases at
367   t=2 s and t=5 s.

368   The first step toward controlling power component effectively is controlling Active and reactive
369   powers. If these components are not controlled accurately, it will not be possible to share other power
370   components effectively. Fig. 12 shows instantaneous real and reactive power components of DG units.
371   Before the t=2 s, all loads in the system are balanced. The rating power of both DGs is the same.
372   Therefore, their share of active and reactive power is the same. Fig. 12 (a) shows the active power
373   output of DG units. As it seems, both units provide the exact amount of active power. Fig. 12 (b) shows
374   the reactive power output of DG units. The reactive power sharing in LV networks is not as accurate as
375   active power component. Since the ratio of reactance to inductance in an LV network is high, usually
376   active and reactive power components are not decoupled effectively. However, the accuracy of reactive
377   power sharing is quite acceptable for this research which its goal is demonstrating unbalanced current
378   sharing in LV networks. Fig. 7 (a) shows the frequency of the system. The droop coefficient is set
379   so that on the no-load situation, the frequency stays at 50 Hz. with the use of conventional droop
380   with a dynamic coefficient, the voltage and frequency reach stable mode after about 0.5 seconds of
381   transient time. Fig. 7 (b) shows the voltage output the at DG1 terminal. After addition of unbalanced
382   load to the loads, a double frequency ripple is added to frequency and voltage of the network. The
383   frequency and voltage deviation is less than 1 and 5 percent for frequency and voltage respectively.
384   Which demonstrate that the deviation is in the range of acceptable limit for frequency and voltage.
385   Figs. 10(a) and (b) show the zero-sequence output impedances and the zero-sequence currents of the
386   DGs, respectively. As it was mentioned earlier, the primary aim of the unbalanced current sharing
387   strategy is to compensate zero- and negative-sequence currents locally. However, if the maximum
388   capacity of a unit to compensate unbalanced currents is reached, other units inject the remaining
389   unbalanced current. Prior to t=5 s, the VZSIC and VNSIC of the DG units are not activated, and virtual
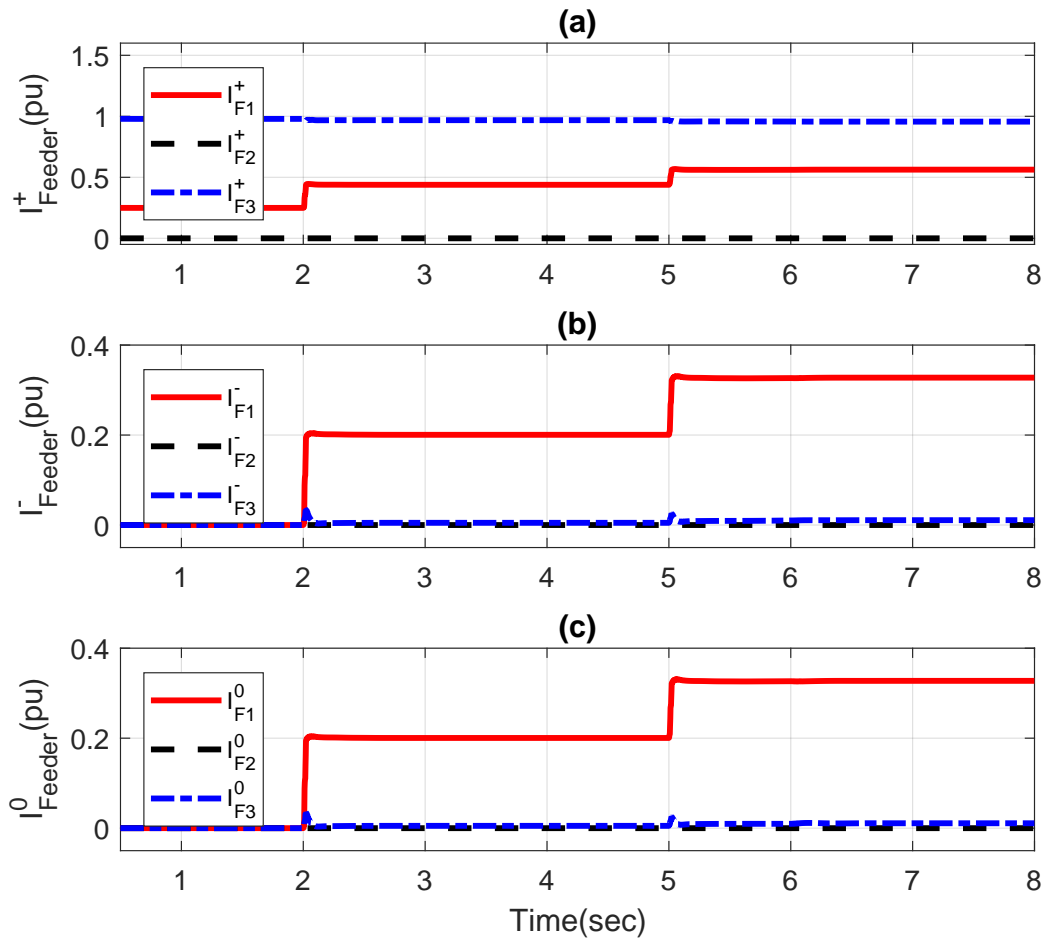
Figure 9. (a) Positive-, (b) negative- and (c) zero-sequence currents of the feeders.
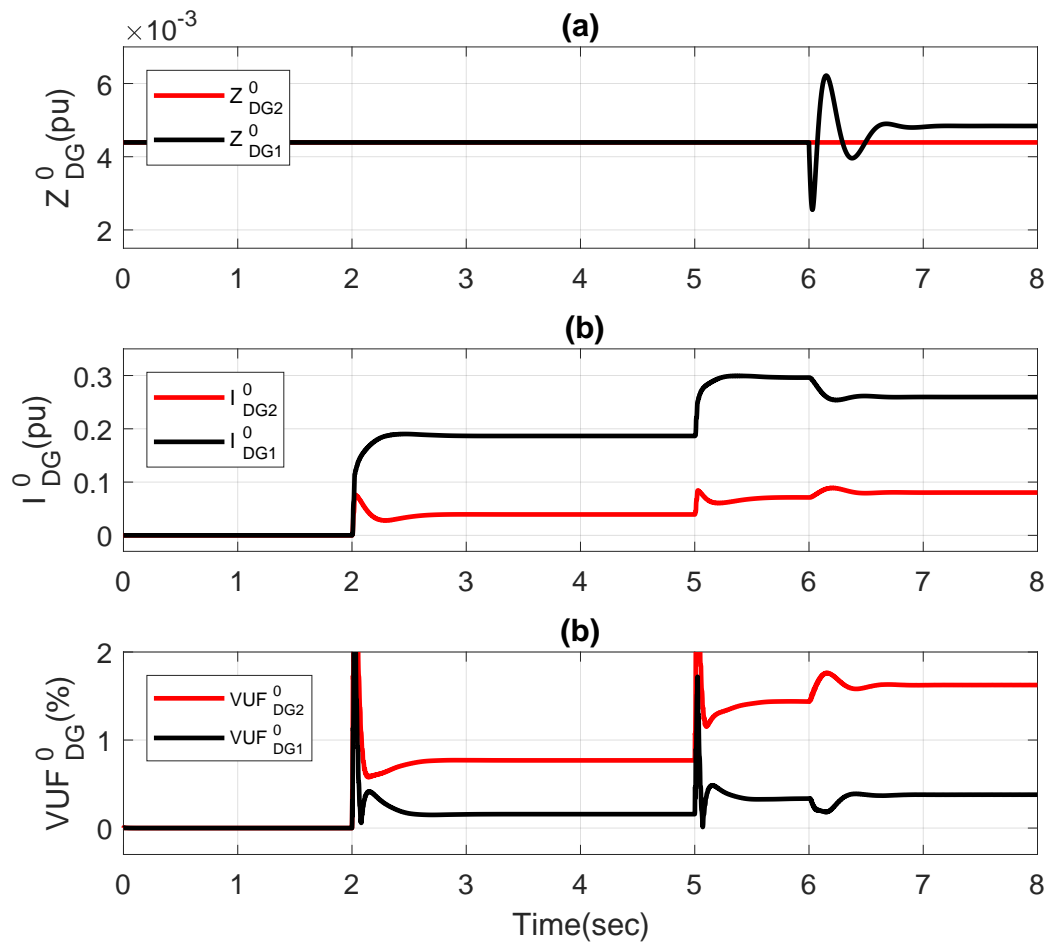
Figure 10. Zero-sequence (a) output impedance, (b) current, and (c) VUF of DG units.

impedances are kept at the minimum value. Fig. 10 (b) shows that almost all zero-sequence current of the unbalanced load is compensated by unit 1. However, when another unbalanced load is added to feeder $F1$ at $t=5$ s, the maximum capacity of the adjacent unit ($DG1$) is reached, and the remaining unbalanced current is then provided by the other unit ($DG2$). This operation is done by increasing the zero-sequence virtual impedance of unit 1 when the VZSIC of unit 1 detects that the maximum capacity of the unit is reached.

Figs. 11 (a) and (b) show the negative-sequence output impedance and the negative-sequence currents of the DGs, respectively. The same scenario happens for negative-sequence current when the maximum capacity of unit 1 for providing negative-sequence current is reached, and the remaining negative-sequence current is shared by another unit through the activation of VNSIC. Fig. 10(C) and Fig. 11(C) show, respectively, the voltage unbalanced factor (VUF) for the zero- and negative-sequence voltage of DG units during load changes. The VUF of $DG1$ is always under 2 percent for zero- and negative-sequences while DG1 is injecting the maximum value of zero- and negative-sequence currents. Fig. 12 shows instantaneous real and reactive power components of DG units. The magnitude of double-frequency ripple on the output power of each unit is proportional to its unbalanced current share.
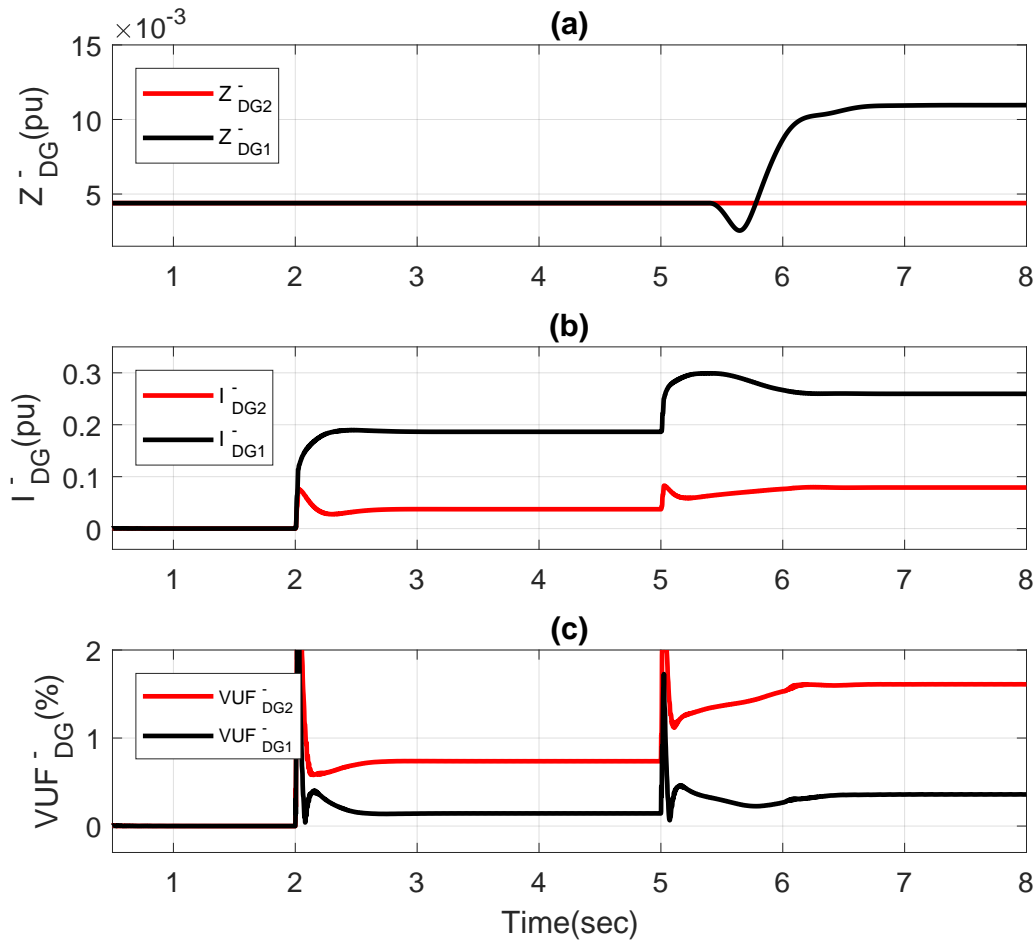
Figure 11. Negative-sequence (a) output impedance, (b) current, and (c) VUF of DG units.

3.2. Case study II

In this case study, the microgrid begins to operate with two balanced loads. The first load is a three-phase 75 kVA with PF=0.9 which is connected to the feeder $F1$ and the second is a 285 kVA with PF=0.88 which is connected to feeder $F3$. Two single-phase loads rated 20 kVA with PF=0.98 are connected to the phase b and c of feeder $F3$ at t=2 s. Subsequently, two single-phase loads are connected to the phase b and c of feeder $F1$ at t=5 s and are disconnected at t=8 s. Then, a single-phase load rated 8 kVA and PF=0.96 is connected to the phase a of feeder $F1$ at t=11 s. Fig. 14 shows the instantaneous real and reactive power components of feeders. When the unbalanced loads are connected to the phase b and c of feeder $F3$, a 100 Hz ripple appears on the power components of feeder $F3$. Furthermore, this ripple appears on the power components of feeder $F1$ when unbalanced loads are connected to it. Fig. 15 shows the positive-, negative- and zero-sequence current components of the feeders. In this case study, loads which are fed from feeder $F3$ have no upstream DG unit. Therefore, unbalanced loads connected to this feeder should be shared by their adjacent units. Fig. 16(a) and Fig. 17(a) show the zero- and negative-sequence virtual impedances of DG units. After the connection of the unbalanced loads to feeder $F3$ at t=2 s, the VZSIC and VNSIC are activated at t=2.4 s. While VZSIC and VNSIC are not activated, the unbalanced load sharing is performed according to the line impedances. Fig. 16(b) and Fig. 17(b) show the zero- and the negative-sequence current components of the DG units, respectively. Having activated the VZSIC and VNSIC of $DG1$, the unbalanced current of feeder $F3$ is shared between DG units according to their negative- and zero-sequence capacities that are considered
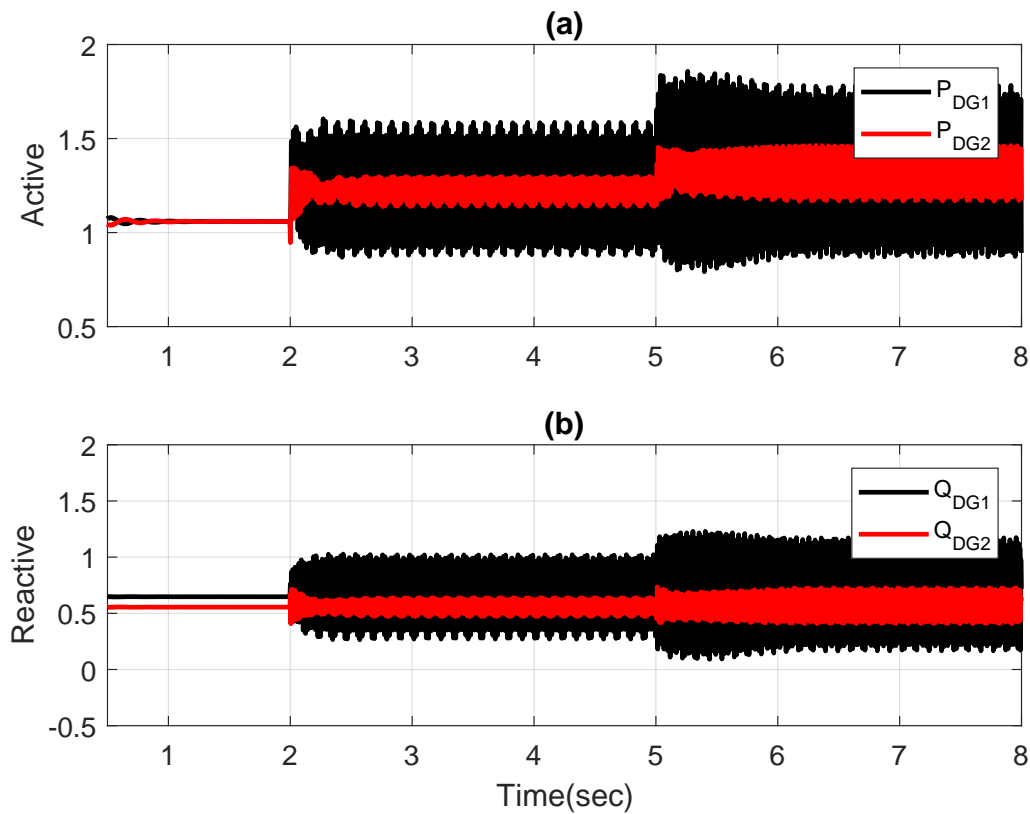
Figure 12. Dynamic response of DG units to unbalanced load changes in feeder F_1: (a) real power, and (b) reactive power components of DG units.

to be equal for units. Therefore, negative- and the zero-sequence current components of units become equal. When the unbalanced load is connected to feeder $F1$ at t=5 s, it should be compensated by unit 1 according to the proposed strategy. Therefore, $DG1$ decreases its Z_V^- and Z_V^0. As it can be seen from Fig. 16(b) and Fig. 17(b), the unbalanced load current flowing through feeder $F1$ at t=5 s is completely compensated by $DG1$ while the portion of unbalanced current injected by $DG2$ is kept intact. At t=8 s, the unbalanced load is disconnected from feeder $F1$. Therefore, VZSIC and VNSIC units of $DG1$ increase Z_V^- and Z_V^0 so that the unbalanced current portion of units become equal. At t=11 s, a single-phase load is connected to the phase a of feeder $F1$. However, this load compensates a portion of the unbalanced load connected to the phase b and c of Feeder $F3$. Therefore, the portion of the unbalanced current supplied by $DG1$ is decreased. The VZSIC and VNSIC increase the virtual impedances to accommodate this situation. If the amplitude of unbalanced current had been only considered ignoring its phase, the calculation of $I_{DG}^-{}^*$ and $I_{DG}^0{}^*$ would have been incorrect causing inaccurate current sharing. Fig. 16(c) and Fig. 17(c) show the voltage unbalanced factor for zero- and negative-sequence voltages. Throughout the simulation time, VUF has a good condition and is always kept under 2 percent.

Fig. 18 shows the output powers of DG units. The double-frequency ripple on the output powers stems from the unbalanced power. When the unbalanced load is connected to the feeder $F3$, the 100 Hz frequency ripple appears in the output power. After t=5 s, the portion of the unbalanced power for $DG1$ increases while the portion of $DG2$ does not change. The unbalanced quota of units become equal after t=8 s. It shows that the control strategy has managed to share the unbalanced power in the microgrid with excellent accuracy.
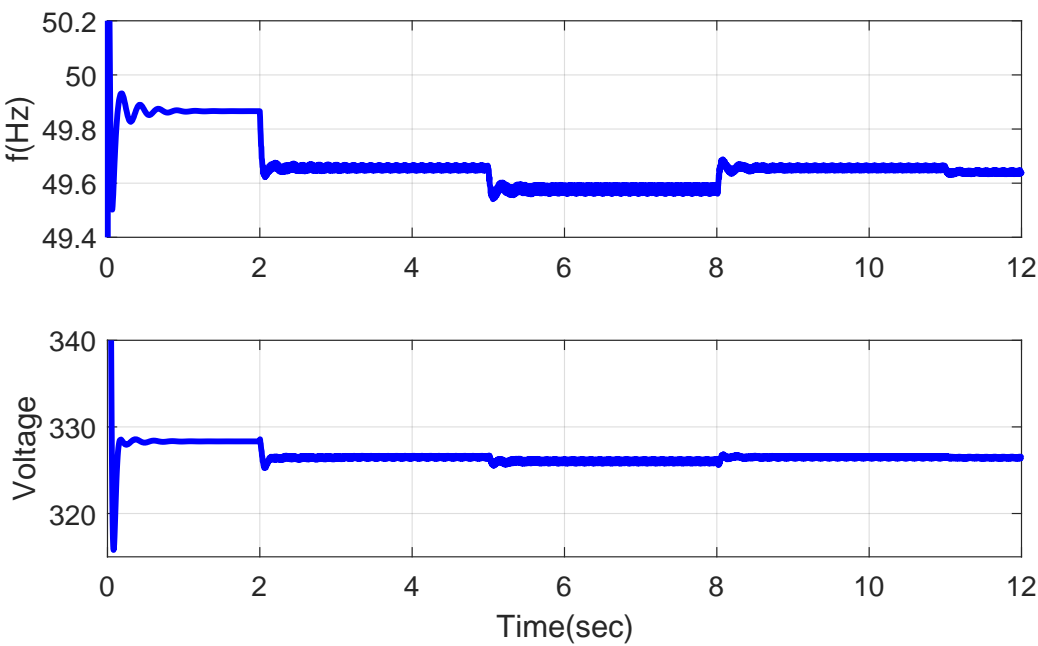
Figure 13. Instantaneous voltages at the DG terminals during unbalanced load changes in feeder F_1, (a) DG_1 and (b) DG_2.
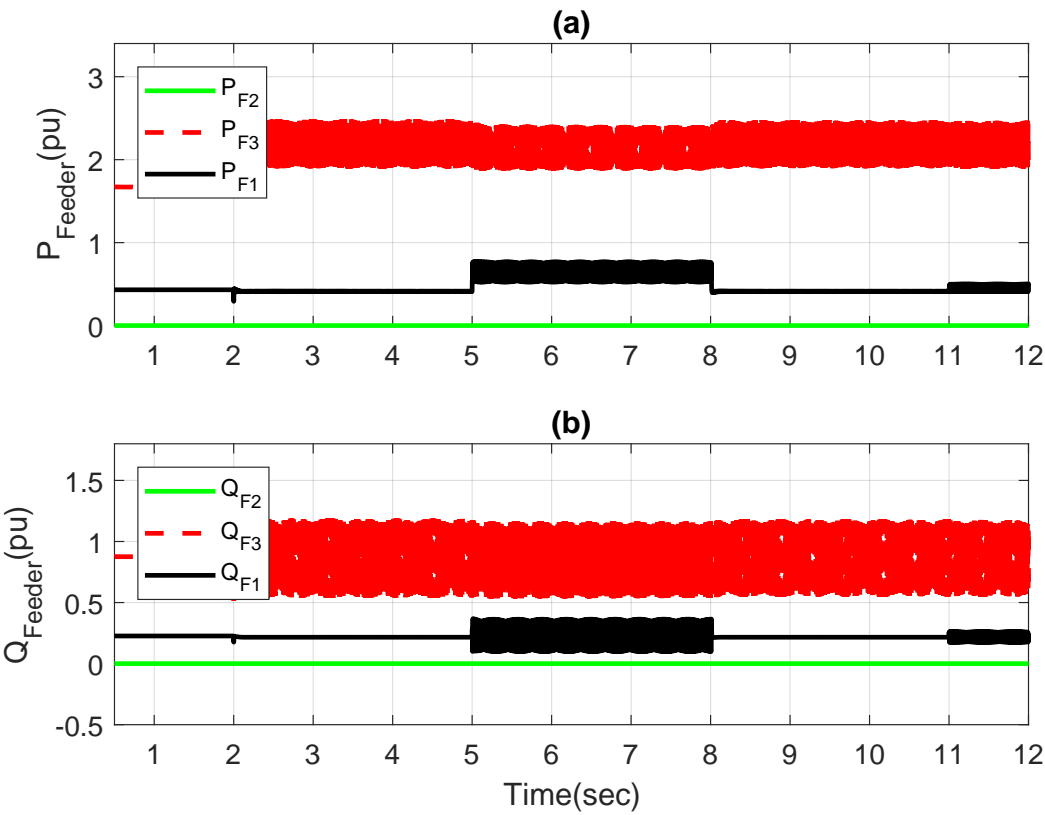
Figure 14. Unbalanced load changes in feeders F_3 and F_2 (a) instantaneous real and (b) reactive power of feeders.
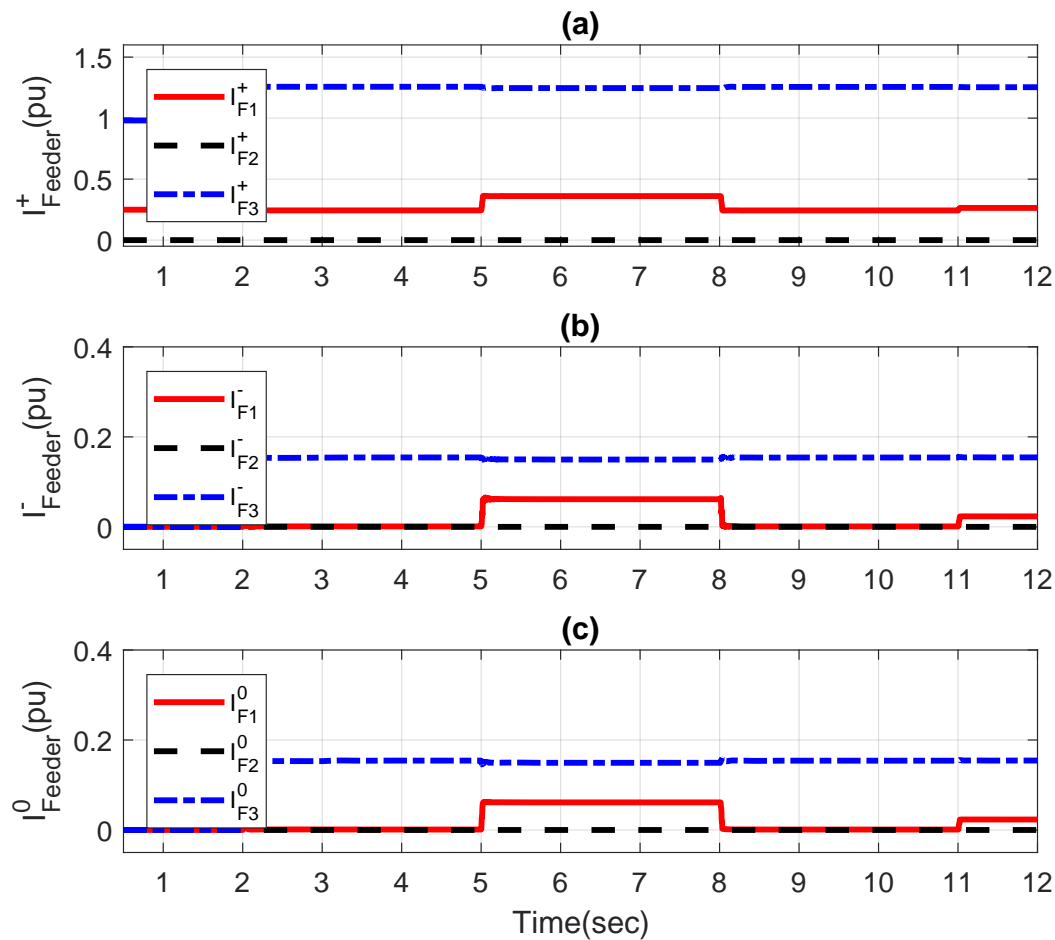
Figure 15. (a) positive and (b) negative, and (c) zero-sequence currents of the feeders.

4. Conclusion

A comprehensive strategy was presented for sharing unbalanced current in an islanded LV microgrid consisting of dispatchable units. In the proposed method, the zero- and negative-sequence currents are shared based on a novel strategy that decreases the flow of unbalanced current in the microgrid improving the overall power quality. In the proposed strategy, the zero- and negative-sequence currents of nonlocal loads are completely compensated by their associated DG units. However, if the capacity of a unit is not enough to offset the zero- and/or negative-sequence current terms or the unbalanced load has no upstream unit, the unbalanced current is shared among adjacent units. The proposed control strategy comprises a PR controller, a droop controller, a virtual negative-sequence impedance controller (VNSIC) and a virtual zero-sequence impedance controller (VZSIC). With VNSIC and VZSIC, the DG units can effectively share the negative- and zero-sequence currents. The performance of the proposed control strategy was evaluated by using digital time-domain simulation studies in PSCAD/EMTDC software. From the simulation results, we found that the proposed control strategy can

- control voltage and frequency while maintaining them within their allowable limits,
- share the average power among DG units, and
- effectively compensates the zero- and negative-sequence currents of unbalanced loads in a four-wired LV microgrid so that the power quality of the overall microgrid is improved.
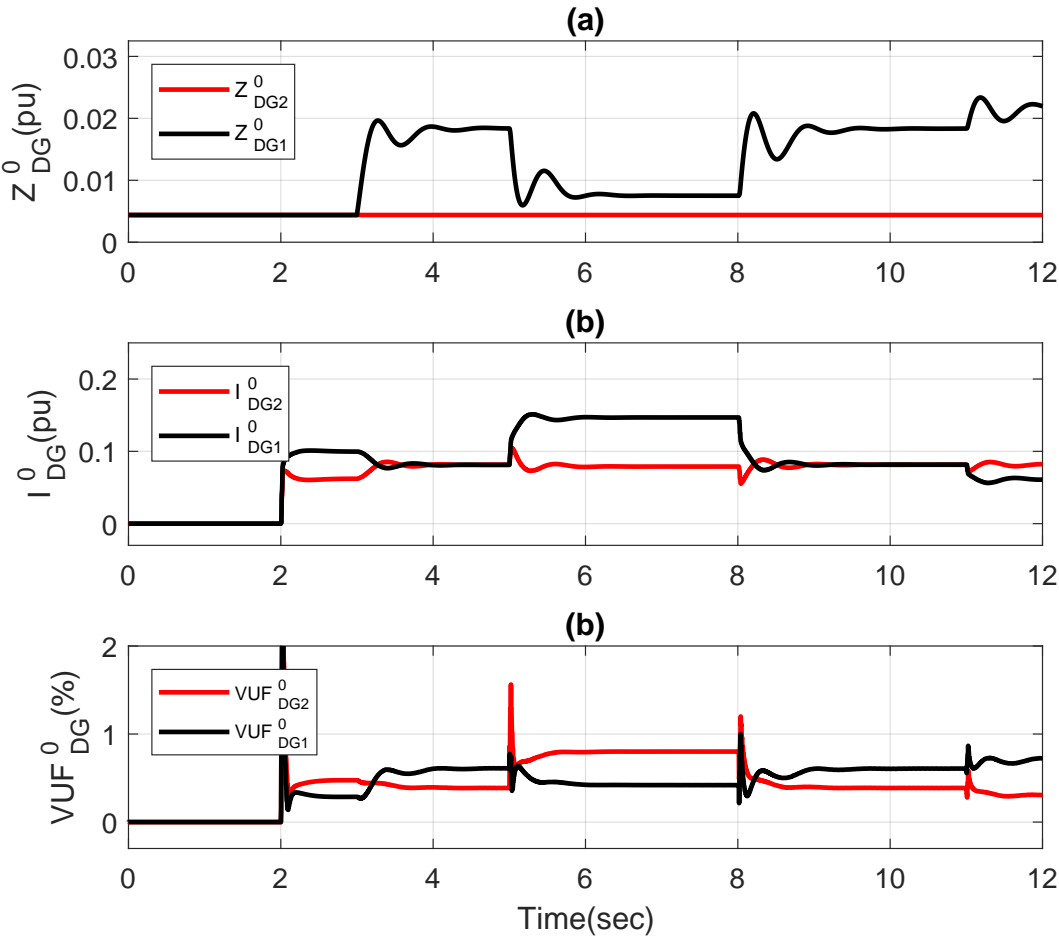
Figure 16. Zero-sequence (a) output impedance, (b) current, and (c) VUF of DG units.

Author Contributions: Conceptualization, F.N. and M.F.; Methodology, F.N. and M.F.; Software, F.N.; Validation, F.N.; Formal Analysis, F.N.; Investigation, F.N.; Resources, M.F.; Data Curation, F.N.; Writing—Original Draft Preparation, F.N. and M.F.; Writing—Review & Editing, F.N. and M.F.; Visualization, F.N.; Supervision, M.F.; Project Administration, M.F.; Funding Acquisition, M.F.

Funding: This research was partly funded by grants from the Ulupono Initiative and Blue Planet Foundation.

Conflicts of Interest: The authors declare no conflict of interest. The funding sponsors had no role in the design of the study; in the collection, analyses, or interpretation of data; in the writing of the manuscript, and in the decision to publish the results.

Abbreviations

The following abbreviations are used in this manuscript:

MDPI Multidisciplinary Digital Publishing Institute
DOAJ Directory of open access journals
TLA   Three letter acronym
LD   linear dichroism

1.   Lasseter, R.; Akhil, A.; Marnay, C.; Stephens, J.; Dagle, J.; Guttromson, R.; Meliopoulous, A.S.; Yinger, R.; Eto, J. Integration of distributed energy resources. The CERTS Microgrid Concept **2002**.
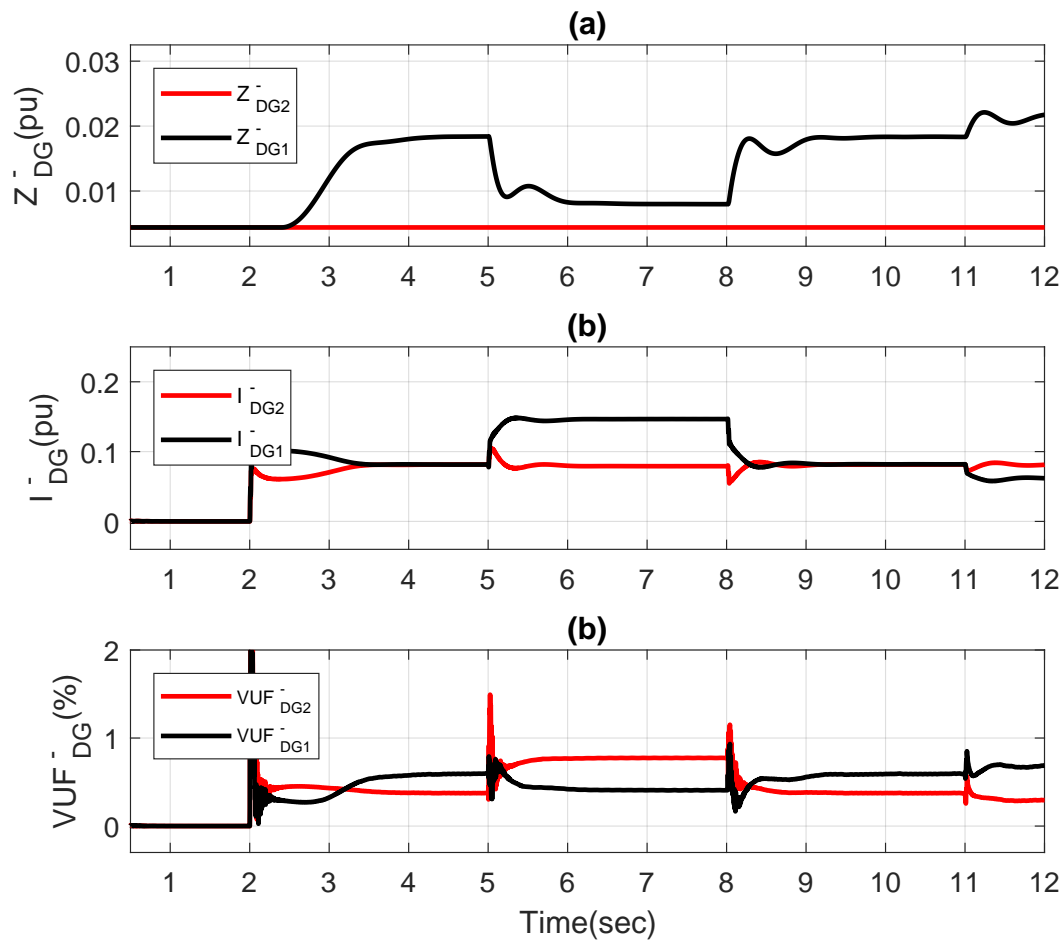
Figure 17. Negative-sequence (a) output impedance, (b) current, and (c) VUF of DG units.

479 2. Coujard, C.; Rodriguez, R.; Bollen, M.; Grenard, S. Innovative training techniques to account for power
480   quality issues when deploying distributed energy resources. *2007 9th International Conference on Electrical*
481   *Power Quality and Utilisation, EPQU* **2007**, pp. 1–6. doi:10.1109/EPQU.2007.4424157.
482 3. Li, B.; Roche, R.; Miraoui, A. Microgrid sizing with combined evolutionary algorithm and MILP unit
483   commitment. *Applied Energy* **2017**, *188*, 547–562. doi:10.1016/j.apenergy.2016.12.038.
484 4. Moradi, M.H.; Foroutan, V.B.; Abedini, M. Power flow analysis in islanded Micro-Grids via modeling
485   different operational modes of DGs: A review and a new approach. *Renewable and Sustainable Energy*
486   *Reviews* **2017**, *69*, 248–262. doi:10.1016/j.rser.2016.11.156.
487 5. Abdelaziz, M.M.; El-Saadany, E. Maximum loadability consideration in droop-controlled
488   islanded microgrids optimal power flow. *Electric Power Systems Research* **2014**, *106*, 168–179.
489   doi:10.1016/j.epsr.2013.08.020.
490 6. Caramia, P.; Carpinelli, G.; Mottola, F.; Russo, G. An optimal control of distributed energy resources to
491   improve the power quality and to reduce energy costs of a hybrid AC-DC microgrid. *IEEE* **2016**, pp. 1–7.
492 7. Mehrasa, M.; Pouresmaeil, E.; Jørgensen, B.N.; Catalão, J.P. A control plan for the stable operation of
493   microgrids during grid-connected and islanded modes. *Electric Power Systems Research* **2015**, *129*, 10–22.
494 8. Mehrasa, M.; Pouresmaeil, E.; Mehrjerdi, H.; Jørgensen, B.N.; Catalão, J.P. Control technique for enhancing
495   the stable operation of distributed generation units within a microgrid. *Energy Conversion and Management*
496   **2015**, *97*, 362–373.
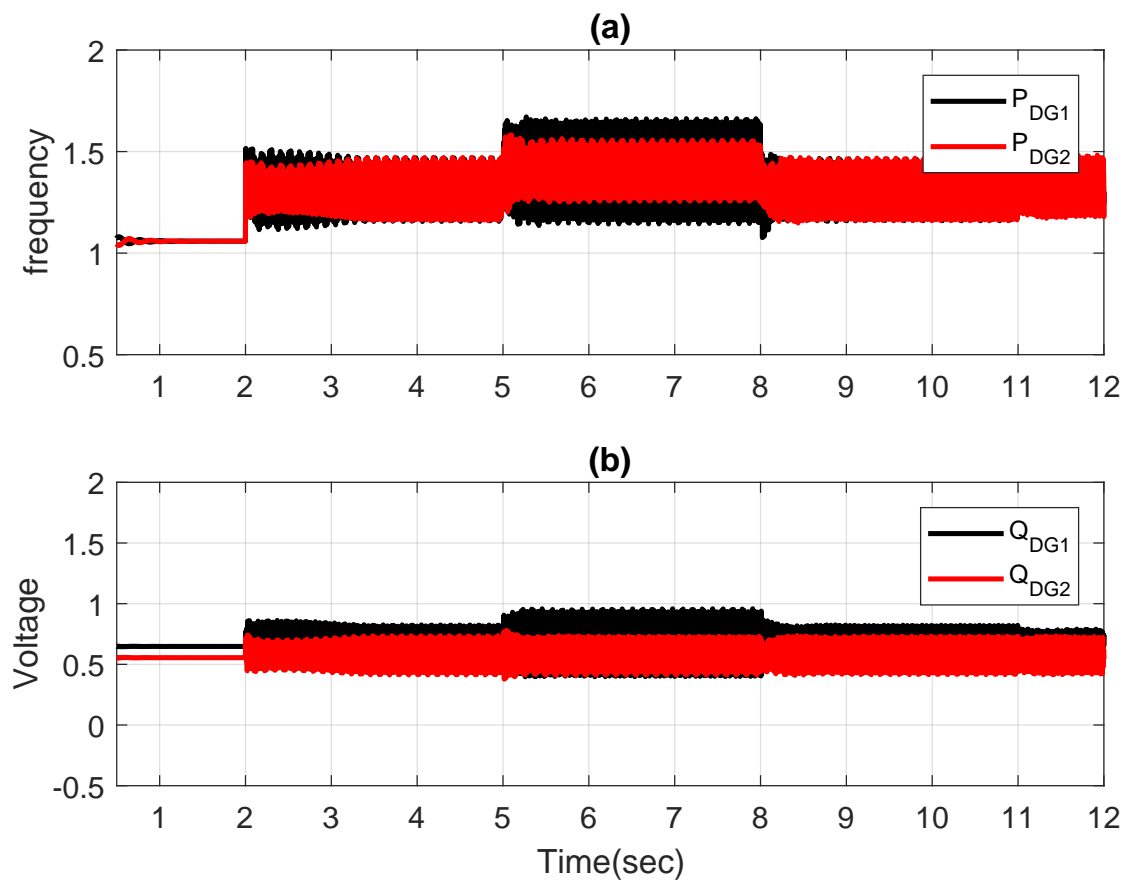
Figure 18. Dynamic response of DG units to unbalanced load changes in feeder F_1 and F_3: (a) real power, and (b) reactive power components of DG units.

9. Shahnia, F.; Chandrasena, R.P.S. A three-phase community microgrid comprised of single-phase energy resources with an uneven scattering amongst phases. *International Journal of Electrical Power and Energy Systems* **2017**, *84*, 267–283. doi:10.1016/j.ijepes.2016.06.010.

10. Palizban, O.; Kauhaniemi, K.; Guerrero, J.M. Microgrids in active network management—Part I: Hierarchical control, energy storage, virtual power plants, and market participation. *Renewable and Sustainable Energy Reviews* **2014**, *36*, 428–439. doi:10.1016/j.rser.2014.01.016.

11. Hochgraf, C.; Lasseter, R.H. Statcom controls for operation with unbalanced voltages. *IEEE Transactions on Power Delivery* **1998**, *13*, 538–544. doi:10.1109/61.660926.

12. Pati2012. Unbalanced Load Compensation **2012**. *1*, 74–80.

13. Sun, Q.; Zhou, J.; Guerrero, J.M.; Zhang, H. Hybrid Three-Phase/Single-Phase Microgrid Architecture With Power Management Capabilities. *IEEE Transactions on Power Electronics* **2015**, *30*, 5964–5977. doi:10.1109/TPEL.2014.2379925.

14. Smith, J.C.; Hensley, G.; Ray, L. IEEE Recommended Practice for Monitoring Electric Power Quality. *IEEE Std* **1995**, pp. 1159–1995.

15. Mehrasa, M.; Pouresmaeil, E.; Jørgensen, B.N.; Catalão, J.P.S. A control plan for the stable operation of microgrids during grid-connected and islanded modes. *Electric Power Systems Research* **2015**, *129*, 10–22. doi:10.1016/j.epsr.2015.07.004.

16. Savaghebi, M.; Jalilian, A.; Vasquez, J.C.; Guerrero, J.M. Secondary Control for Voltage Quality Enhancement in Microgrids. *IEEE Transactions on Smart Grid* **2012**, *3*, 1893–1902. doi:10.1109/TSG.2012.2205281.

17. Delghavi, M.B.; Yazdani, A. Islanded-mode control of electronically coupled distributed-resource units under unbalanced and nonlinear load conditions. *IEEE Transactions on Power Delivery* **2011**, *26*, 661–673.

18. Quan, X.; Dou, X.; Wu, Z.; Hu, M.; Yuan, J. Harmonic voltage resonant compensation control of a three-phase inverter for battery energy storage systems applied in isolated microgrid. *Electric Power Systems Research* **2016**, *131*, 205–217. doi:10.1016/j.epsr.2015.10.010.

19. Saim, A.; Mellah, R.; Houari, A.; Machmoum, M.; Djerioui, A. Adaptive resonant based multi-loop control strategy for parallel distributed generation units in standalone microgrid application. *Electric Power Systems Research* **2017**, *143*, 262–271. doi:10.1016/j.epsr.2016.10.010.

20. Abdelaziz, M.M.A.; El-Saadany, E.F. Economic droop parameter selection for autonomous microgrids including wind turbines. *Renewable Energy* **2015**, *82*, 108–113. doi:10.1016/j.renene.2014.09.024.

21. Li, J.; Xiong, R.; Yang, Q.; Liang, F.; Zhang, M.; Yuan, W. Design/test of a hybrid energy storage system for primary frequency control using a dynamic droop method in an isolated microgrid power system. *Applied Energy* **2016**. doi:10.1016/j.apenergy.2016.10.066.

22. Oureilidis, K.O.; Demoulias, C.S. A decentralized impedance-based adaptive droop method for power loss reduction in a converter-dominated islanded microgrid. *Sustainable Energy, Grids and Networks* **2016**, *5*, 39–49. doi:10.1016/j.segan.2015.11.003.

23. Rezaei, M.M.; Soltani, J. A robust control strategy for a grid-connected multi-bus microgrid under unbalanced load conditions. *International Journal of Electrical Power and Energy Systems* **2015**, *71*, 68–76. doi:10.1016/j.ijepes.2015.02.041.

24. Hurtt, J.; Mili, L. Residential microgrid model for disaster recovery operations. PowerTech (POWERTECH), 2013 IEEE Grenoble. IEEE, 2013, pp. 1–6.

25. Sao, C.; Lehn, P. Autonomous Load Sharing of Voltage Source Converters. *IEEE Transactions on Power Delivery* **2005**, *20*, 1009–1016. doi:10.1109/TPWRD.2004.838638.

26. Mohamed, Y.; El-Saadany, E. Adaptive Decentralized Droop Controller to Preserve Power Sharing Stability of Paralleled Inverters in Distributed Generation Microgrids. *IEEE Transactions on Power Electronics* **2008**, *23*, 2806–2816. doi:10.1109/TPEL.2008.2005100.

27. Engler, A. Applicability of droops in low voltage grids. *International Journal of Distributed Energy Resources* **2005**, *1*, 1–6.

28. Engler, A.; Osika, O.; Barnes, M.; Hatziargyriou, N. DB2 Evaluation of the local controller strategies. *European Commission: Brussels, Belgium* **2005**.

29. Tuladhar, A.; Jin, H.; Unger, T.; Mauch, K. Parallel operation of single phase inverter modules with no control interconnections. Applied Power Electronics Conference and Exposition, 1997. APEC'97 Conference Proceedings 1997., Twelfth Annual. IEEE, 1997, Vol. 1, pp. 94–100.

30. Guerrero, J.M.; Hang, L.; Uceda, J. Control of distributed uninterruptible power supply systems. *IEEE Transactions on Industrial Electronics* **2008**, *55*, 2845–2859.

31. Kim, J.; Guerrero, J.M.; Rodriguez, P.; Teodorescu, R.; Nam, K. Mode adaptive droop control with virtual output impedances for an inverter-based flexible AC microgrid. *IEEE Transactions on power electronics* **2011**, *26*, 689–701.

32. Jin, P.; Li, Y.; Li, G.; Chen, Z.; Zhai, X. Optimized hierarchical power oscillations control for distributed generation under unbalanced conditions. *Applied Energy* **2016**. doi:10.1016/j.apenergy.2016.06.075.

33. Shahnia, F.; Majumder, R.; Ghosh, A.; Ledwich, G.; Zare, F. Operation and control of a hybrid microgrid containing unbalanced and nonlinear loads. *Electric Power Systems Research* **2010**, *80*, 954–965. doi:10.1016/j.epsr.2010.01.005.

34. Carpinelli, G.; Mottola, F.; Proto, D.; Varilone, P. Minimizing unbalances in low-voltage microgrids: Optimal scheduling of distributed resources. *Applied Energy* **2017**, *191*, 170–182. doi:10.1016/j.apenergy.2017.01.057.

35. Salmerón Revuelta, P.; Pérez Litrán, S.; Prieto Thomas, J.; Salmerón Revuelta, P.; Pérez Litrán, S.; Prieto Thomas, J. 4 – Shunt Active Power Filters. In *Active Power Line Conditioners*; Academic Press, 2016; pp. 107–147. doi:10.1016/B978-0-12-803216-9.00004-3.

36. Jayachandran, J.; Murali Sachithanandam, R. ANN based controller for three phase four leg shunt active filter for power quality improvement. *Ain Shams Engineering Journal* **2016**, *7*, 275–292. doi:10.1016/j.asej.2015.03.007.

37. Golsorkhi, M.S.; Lu, D.D.C. A Decentralized Control Method for Islanded Microgrids under Unbalanced Conditions. *IEEE Transactions on Power Delivery* **2016**, *31*, 1112–1121. doi:10.1109/TPWRD.2015.2453251.

38. Blaabjerg, F.; Teodorescu, R.; Liserre, M.; Timbus, A. Overview of Control and Grid Synchronization for Distributed Power Generation Systems. *IEEE Transactions on Industrial Electronics* **2006**, *53*, 1398–1409. doi:10.1109/TIE.2006.881997.

39. Guerrero, J.; GarciadeVicuna, L.; Matas, J.; Castilla, M.; Miret, J. Output Impedance Design of Parallel-Connected UPS Inverters With Wireless Load-Sharing Control. *IEEE Transactions on Industrial Electronics* **2005**, *52*, 1126–1135. doi:10.1109/TIE.2005.851634.

40. Zhang, Y.; Yu, M.; Liu, F.; Kang, Y. Instantaneous Current Sharing Control Strategy for Parallel Operation of UPS Modules Using Virtual Impedance. *IEEE Transactions on Power Electronics* **2011**, *28*, 432–440.

41. Shah, S.; Sensarma, P.S. Three Degree of Freedom Robust Voltage Controller for Instantaneous Current Sharing Among Voltage Source Inverters in Parallel. *IEEE Transactions on Power Electronics* **2010**, *25*, 3003–3014. doi:10.1109/TPEL.2010.2050150.

42. Kay-Soon Low.; Runzi Cao. Model Predictive Control of Parallel-Connected Inverters for Uninterruptible Power Supplies. *IEEE Transactions on Industrial Electronics* **2008**, *55*, 2884–2893. doi:10.1109/TIE.2008.918474.

43. Harnefors, L.; Bongiorno, M.; Lundberg, S. Input-Admittance Calculation and Shaping for Controlled Voltage-Source Converters. *IEEE Transactions on Industrial Electronics* **2007**, *54*, 3323–3334. doi:10.1109/TIE.2007.904022.

44. Yun Wei Li.; Ching-Nan Kao. An Accurate Power Control Strategy for Power-Electronics-Interfaced Distributed Generation Units Operating in a Low-Voltage Multibus Microgrid. *IEEE Transactions on Power Electronics* **2009**, *24*, 2977–2988. doi:10.1109/TPEL.2009.2022828.

45. De, D.; Ramanarayanan, V. Decentralized Parallel Operation of Inverters Sharing Unbalanced and Nonlinear Loads. *IEEE Transactions on Power Electronics* **2010**, *25*, 3015–3025. doi:10.1109/TPEL.2010.2068313.

46. Xiongfei Wang.; Blaabjerg, F.; Zhe Chen. Autonomous Control of Inverter-Interfaced Distributed Generation Units for Harmonic Current Filtering and Resonance Damping in an Islanded Microgrid. *IEEE Transactions on Industry Applications* **2014**, *50*, 452–461. doi:10.1109/TIA.2013.2268734.

47. Cheng, P.T.; Chen, C.A.; Lee, T.L.; Kuo, S.Y. A Cooperative Imbalance Compensation Method for Distributed-Generation Interface Converters. *IEEE Transactions on Industry Applications* **2009**, *45*, 805–815. doi:10.1109/TIA.2009.2013601.

48. Guerrero, J.; Matas, J.; Garcia De Vicunagarcia De Vicuna, L.; Castilla, M.; Miret, J. Wireless-Control Strategy for Parallel Operation of Distributed-Generation Inverters. *IEEE Transactions on Industrial Electronics* **2006**, *53*, 1461–1470. doi:10.1109/TIE.2006.882015.

49. Kim, J.; Guerrero, J.M.; Rodriguez, P.; Teodorescu, R.; Nam, K. Mode Adaptive Droop Control With Virtual Output Impedances for an Inverter-Based Flexible AC Microgrid. *IEEE Transactions on Power Electronics* **2011**, *26*, 689–701. doi:10.1109/TPEL.2010.2091685.

50. Lee, T.L.; Cheng, P.T. Design of a New Cooperative Harmonic Filtering Strategy for Distributed Generation Interface Converters in an Islanding Network. *IEEE Transactions on Power Electronics* **2007**, *22*, 1919–1927. doi:10.1109/TPEL.2007.904200.

51. Hamzeh, M.; Karimi, H.; Mokhtari, H. Harmonic and Negative-Sequence Current Control in an Islanded Multi-Bus MV Microgrid. *Smart Grid, IEEE Transactions on* **2013**, *PP*, 1.

52. Rowe, C.N.; Summers, T.J.; Betz, R.E.; Cornforth, D.J.; Moore, T.G. Arctan Power–Frequency Droop for Improved Microgrid Stability. *IEEE Transactions on Power Electronics* **2013**, *28*, 3747–3759. doi:10.1109/TPEL.2012.2230190.

53. Hamzeh, M.; Karimi, H.; Mokhtari, H. A New Control Strategy for a Multi-Bus MV Microgrid Under Unbalanced Conditions. *IEEE Transactions on Power Systems* **2012**, *27*, 2225–2232. doi:10.1109/TPWRS.2012.2193906.

54. Guerrero, J.; GarciadeVicuna, L.; Matas, J.; Castilla, M.; Miret, J. Output Impedance Design of Parallel-Connected UPS Inverters With Wireless Load-Sharing Control. *IEEE Transactions on Industrial Electronics* **2005**, *52*, 1126–1135. doi:10.1109/TIE.2005.851634.

55. Hamzeh, M.; Karimi, H.; Mokhtari, H. Harmonic and Negative-Sequence Current Control in an Islanded Multi-Bus MV Microgrid. *IEEE Transactions on Smart Grid* **2014**, *5*, 167–176. doi:10.1109/TSG.2013.2263842.

56.   Ghazanfari, A.; Hamzeh, M.; Mokhtari, H.; Karimi, H. Active power management of multi-hybrid fuel cell/supercapacitor power conversion system in a medium voltage microgrid. *IEEE Trans. On Smart Grids* **2012**, *3*, 1903–1910.

57.   Akagi, H.; Watanabe, E.H.; Aredes, M. *Instantaneous Power Theory and Applications to Power Conditioning*; Wiley, 2007.

58.   Hamzeh, M.; Karimi, H.; Mokhtari, H.; Mahseredjian, J. Control of a microgrid with unbalanced loads using virtual negative-sequence impedance loop. The 5th Annual International Power Electronics, Drive Systems and Technologies Conference (PEDSTC 2014). IEEE, 2014, pp. 78–83. doi:10.1109/PEDSTC.2014.6799348.

59.   Chandorkar, M.; Divan, D.; Adapa, R. Control of parallel connected inverters in standalone AC supply systems. *IEEE Transactions on Industry Applications* **1993**, *29*, 136–143. doi:10.1109/28.195899.

60.   Karimi, H.; Yazdani, A.; Iravani, R. Negative-Sequence current injection for fast islanding detection of a distributed resource unit. *IEEE Transactions On Power Electronics* **2008**, *23*, 298–307.

61.   Cooper, C. IEEE recommended practice for electric power distribution for industrial plants. *Electronics and Power* **1987**, *33*, 658.